# Synergistic effects of hexagonal boron nitride nanoparticles and phosphonium ionic liquids as hybrid lubricant additives

**Khodor I. Nasser, José M. Liñeira del Río, Enriqueta R. López*, Josefa Fernández**

Laboratory of Thermophysical Properties, Nafomat Group, Department of Applied Physics, Faculty of Physics, University of Santiago de Compostela, 15782, Santiago de Compostela, Spain

*Journal of Molecular Liquids 311 (2020) 113343*

https://doi.org/10.1016/j.molliq.2020.113343

*Corresponding author

E-mail address: enriqueta.lopez@usc.es

## Abstract

Hybrid nanostructure combinations of ionic liquids (ILs) and hexagonal boron nitride (h-BN) nanosheets are proposed as additives to lubricants to enhance their tribological performance and their temporal stability. Trihexyltetradecylphosphonium bis(2-ethylhexyl)phosphate (IL1), tributylethylphosphonium diethylphosphate (IL2) and trihexyltetradecylphosphonium bis(2,4,4-trimethylpentyl)phosphinate (IL3) are the ILs (at 1 wt%) that have been combined, each separately, with h-BN nanosheets (at 0.1 wt%), were added as hybrid additives in a polyalphaolefin base lubricant, PAO 32. Some of the nanodispersions remain stable up to 240 days after preparation. Increases in both viscosity and density owing to h-BN nanoparticles and/or ILs are lower than 7 % and 0.3 %, respectively. The tribological performance (friction and wear) of the several developed nanolubricants were investigated using a tribometer with a ball-on-three-pin configuration and a 3D optical profiler, respectively. The results showed that the hybrid additives improve, in general, the tribological performance of the lubricant rather than being used separately, thus synergistic effects have been found. Raman spectroscopy conducted on the worm surface showed protective IL and h-BN tribofilms. PAO 32 + IL1 + h-BN is the nanolubricant that exhibits the best tribological performance of those studied in this work.



**Keywords:** ionic liquids, nanoadditives, friction, wear

## 1. Introduction

Renewable energy sources, including wind, solar or hydropower resources, among others, are widely considered as strategic alternative opportunities for the development of more efficient and reasonable economic systems. Wind energy maximum net generating capacity rose by more than 450 percent over the ten years previous to 2016 [1]. Taking into consideration the high initial costs of building energy systems, it is evident that the failure of any lubricated mechanical component leads to a significant drop of the overall system efficiency, which in turn results in (increased) repair expenses and production breakdown.

Many factors can affect the wind energy system performance, such as climate and location [2, 3]. Several mechanical systems of any wind energy system should be lubricated to reduce both friction and wear between two solid surfaces in contact. Lubricant improvements are always needed to reduce the mechanical failures being the gearbox the component of the wind turbine for which the repair and maintenance costs are higher [4]. Polyalphaolefin oils (PAOs) are the most widely used lubricant bases in wind turbine gearboxes systems [5-7]. PAOs are usually named by their kinematic viscosity in centistokes (cSt) at 373.15 K. For wind turbine gearboxes the most used PAO is PAO 32.

Ionic liquids (ILs) and nanoparticles have been investigated by several researchers as anti-friction and anti-wear additives for several types of oils [4-6, 8-12]. Ionic liquids (ILs) can be considered as organic salts with a low melting point, which is often below room temperature and typically consists of a combination between an anion and a cation. ILs are being investigated for either lubricant or as additives in oils due to their ability to reduce friction and wear to enhance machine behavior [9-11]. Due their inherent polarity, ILs form effective physical adsorption films and promote tribo-chemical reaction films onto the sliding surfaces. Both effects could reduce friction and wear on the steel surface [13]. Nanoparticles (NPs), including nanocrystals, nanoclusters, nanometals, nanotubes, … are materials with different shapes and

68 properties used in biological, medical and engineering applications [14, 15] as lubricant additives
69 [8, 12, 16, 17].

70 ILs are excellent dispersants for the stabilization of well-characterized nanomaterials. The
71 IL/NP hybrid combinations have potential as lubricants or lubricant additives, in the latter case,
72 especially for conventional lubricants where these nanomaterials might not be readily
73 dispersible [18-21]. Several hybrid structures composed by ILs and NPs can be formed depending
74 on a balance of intra- and inter-molecular interactions between them [22]. Very few of these
75 hybrid structures were tested as additives of base oils, demonstrating synergistic effects in
76 reduction of friction and wear, as well as an increase in the temporal stability of dispersions [21,
77 23-27]. Thus, ILs can form layers around the NPs preventing aggregation [22], which result in the
78 improvement of the system efficiency and performance. The tribological performance of the
79 hybrid nanolubricant is not only related to the types of the ILs and the NPs dispersed in the oil,
80 but also the homogenization and the stability are important aspects to be considered.

81 Fan and Wang [23] have studied high-performance lubricant additives, based on modified
82 graphene oxide by ionic liquids, for multialkylated cyclopentanes. Excellent tribological
83 properties attributed to the formation of an ILs-containing graphene-rich tribofilm on the sliding
84 surfaces were found. As regards hybrid additives for PAO oils, only Seymour *et al.* [26]
85 investigated hairy Silica NPs and a phosphonium-phosphate IL dispersed in PAO 4, finding better
86 tribological behavior using the hybrid combination rather than the IL and NPs separately as
87 additives in the base oil. Regarding polyethylene glycol (PEG) base oils, Li *et al.* [24] reported
88 synergistic lubrication effects of 2-mercaptobenzothiazolate based ILs and Mo NPs as hybrid
89 additives, demonstrating that the hybrid oil performance for friction-reduction and anti-wear
90 was better at 373.15 K rather than at 293.15 K. For palm olein trimethylolpropane ester (MRPO),
91 Amiril *et al.* [28] concluded that there was no positive antifriction synergy between hexagonal
92 boron nitride (h-BN) NPs and a phosphonium ionic liquid. Sanes *et al.* [21] studied the synergies
93 between graphene and ionic liquid lubricant additives for both an isoparaffinic base oil and a

fully formulated oil. They encountered a friction reduction of 33% and a remarkable decrease of the wear in the first case whereas for the formulated oil the hybrid additive does not lead to better antifriction behavior than graphene. Liñeira del Río *et al.* [25] analyzed the synergies of an IL and h-BN or graphene nanoplatelets (GnP) in a trimellitate base oil concluding that the best antifriction (33%) and antiwear (44% for the track width) performance corresponds to the IL/GnP hybrid additive. Finally, Upendra and Vasu [27] studied the tribological properties of the IL trihexyltetradecylphosphonium bis(2,4,4-trimethylpentyl) phosphinate along with $Al_2O_3$, CuO, and $SiO_2$ nanoparticles (NPs) as hybrid additives in a group I mineral base oil. Improved triboperformances due to the formation of a tribofilm rich in phosphate and tribosintered NPs on the worn surface were found.

In this work, an investigation of three phosphonium ILs with h-BN NPs as hybrid additives for PAO 32 base oil at a steel to steel contact have been carried out. PAO 32 was selected because it is used as the base oil of formulated lubricants in wind turbine gearboxes. h-BN is an environmentally friendly material whose nanosheets have shown excellent behavior as an additive of other base oils [29, 30]. Phosphonium based ILs have shown both better miscibility and excellent tribological performance as additives of current lubricants compared with most ILs. [11, 31]. The synergistic effects between these additives on lubrication performance were analyzed in terms of friction and wear. According to Coronado and Wenske [32], oil temperature of wind turbines is under 353.15 K, Sequeira *et al.* [33] concluded that the optimum temperature for gearbox oils ranges between 318.15 and 338.15 K, but temperature peaks of around 353 K can occur [34]. In addition, the gearboxes do not start to operate if the temperature of the lubricant is not higher than 300 K. For this reason, we have selected the temperatures 298.15 K and 353.15 K to evaluate the tribological behavior at the extrema of the temperature range. These results can assist in identifying the hybrid lubricant additives on oil performance which lead to the development of

new formulated lubricants. For better characterization of the hybrid lubricants, thermophysical properties, density and dynamic viscosity, have been measured. In addition, corrosion tests of the ILs on smooth steel surfaces were performed.

## 2. Experimental section

### *2.1. Materials*

The ionic liquids trihexyltetradecylphosphonium bis(2-ethylhexyl)phosphate (IL1), Tributylethylphosphonium diethylphosphate (IL2) and trihexyltetradecylphosphonium bis(2,4,4-trimethylpentyl)phosphinate (IL3) were supplied by Iolitec. The purities and the CAS numbers of the ILs are reported in Table 1. No further purification was performed for these ILs.

**Table 1**

Main information of materials used in this work.

| Chemical name | Reduced name | Supplier | CAS number | Purity* |
|---|---|---|---|---|
| PAO 32 | PAO 32 | REPSOL | 533903-84-3 | |
| Hexagonal boron nitride nanoparticles | h-BN | Iolitec | 10043-11-5 | 0.995 |
| trihexyltetradecylphosphonium bis(2-ethylhexyl)phosphate (IL1) | $[P_{6,6,6,14}][DEHP]$ | Iolitec | 1092655-30-5 | >0.98 |
| Tributylethylphosphonium diethylphosphate (IL2) | $[P_{2,4,4,4}][DEP]$ | Iolitec | 20445-94-7 | >0.95 |
| trihexyltetradecylphosphonium bis(2,4,4-trimethylpentyl)phosphinate (IL3) | $[P_{6,6,6,14}][(iC8)_2PO_2]$ | Iolitec | 465527-58-6 | >0.9 |

* Given by the supplier

Hexagonal boron nitride (h-BN) nanoparticles were also supplied by Iolitec, with a mole fraction purity of 0.995 (lot MNC018001), a nominal diameter of 70 nm and a bulk density of 2.29 g/cm$^3$. Scanning Electron Microscope (SEM) micrographs, transmission electron microscope (TEM) images, X-ray patterns, Fourier-transform infrared (FTIR) spectrum, Raman spectrum and EDX microanalyses of the h-BN nanoparticles were previously reported by Liñeira

del Río *et al.* [29] and Guimarey *et al.* [35] where the EDX results show that purity is approximately 99%.

Polyalphaolefin 32 (PAO 32), supplied by REPSOL, is a mixture of PAO 40 (89 wt%) and PAO 6 (11 wt%), which are chemically synthetized by the hydrogenation of polymerized 1-decene. PAO 32 and the three ILs were analyzed by Fourier transform infrared spectrometry (FTIR, VARIAN 670-IR). The FTIR spectrum for PAO 32 (Figure 1) shows the following peaks: a band with two intense peaks at (2852 and 2920) $cm^{-1}$ corresponding to C–H stretching vibrations of the aliphatic carbon chain, other band with two moderate peaks at (1377 and 1462) $cm^{-1}$ due to the C–H deformation of the aliphatic group $–CH_3$ [35, 36] and a vibration signal at 721 $cm^{-1}$ which can be attributed to in-plane bending or rocking of the methylene groups ($–CH_2–$) [37, 38]. These peaks are almost identical to those obtained previously by Guimarey *et al.* [35] for PAO 6 and by Liñeira del Río *et al.* [38] for PAO 40.

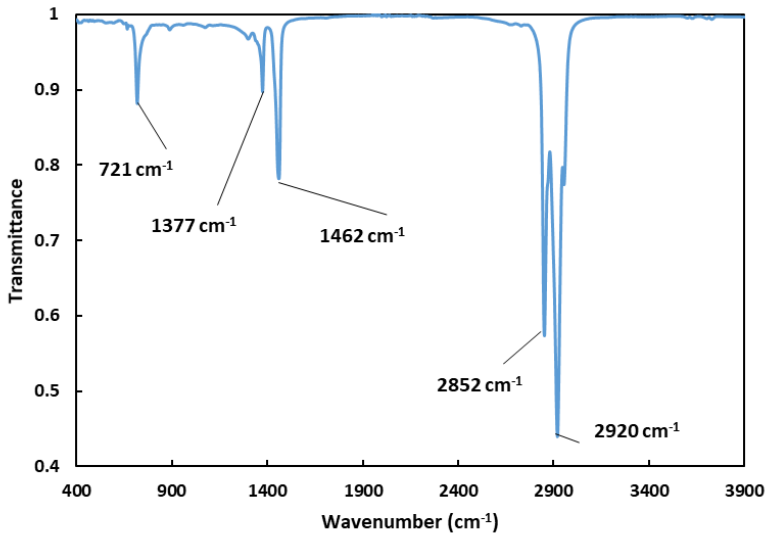


**Fig. 1.** FTIR spectrum of the base oil PAO 32.

The FTIR spectra of the three ILs are shown in Figure 2. As can be observed, the FTIR bands of PAO 32 also exist in the FTIR spectra of the three ILs, due to the presence of alkyl chains. Moreover, a peak between 1229 and 1249 $cm^{-1}$, depending on the IL, corresponding to the anion P=O bond stretch [39, 40] is presented. In addition, for IL3 a strong peak at 1170 $cm^{-1}$ which is also characteristic to a P=O bond stretch [39].

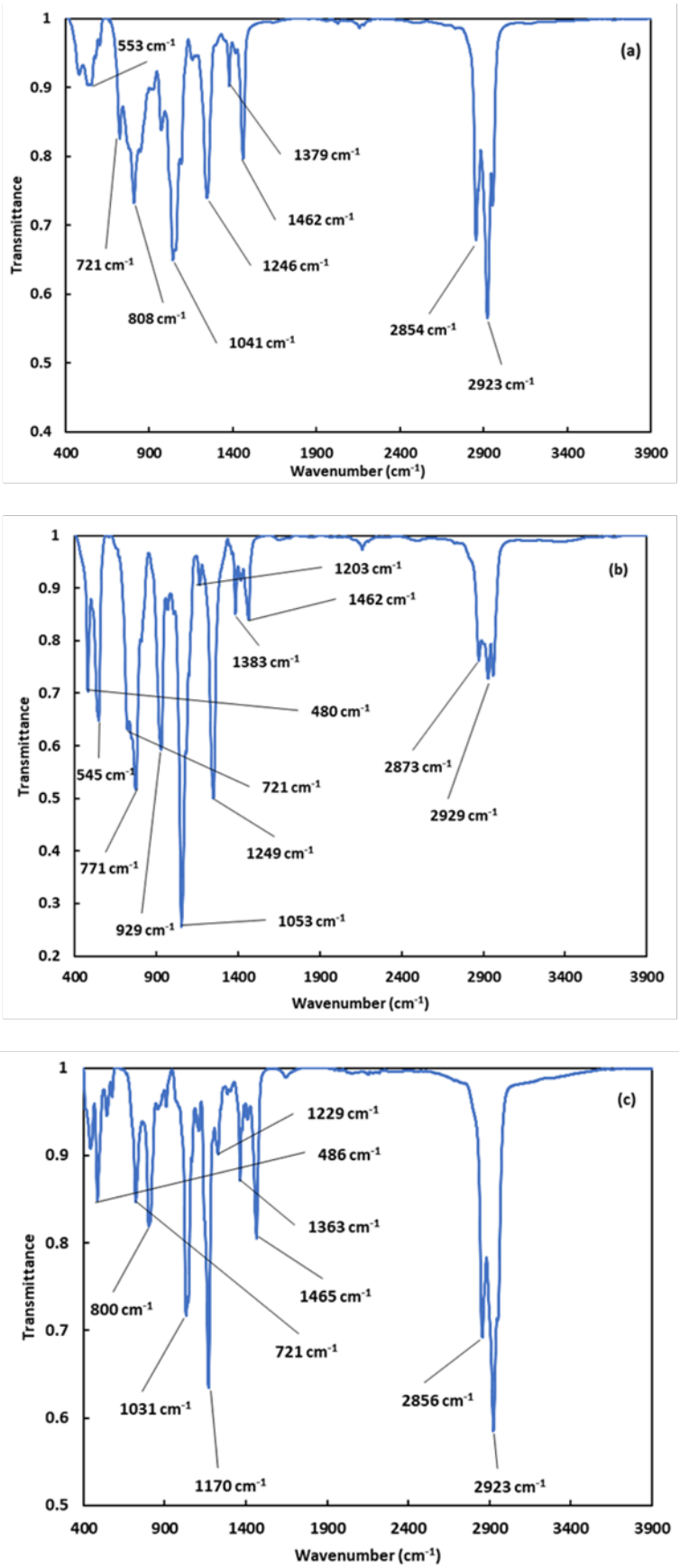


**Fig. 2.** FTIR spectra of: (a) IL1, (b) IL2 and (c) IL3

A WITec alpha300R+ confocal Raman microscope was employed to obtain the Raman spectrum of PAO 32 and the three ILs. As can be observed in Figure S1 and S2, a Raman band is detected around 2800-3000 $cm^{-1}$ with peaks at 2857 and 2908, 2909 and 2930 $cm^{-1}$ assignable to C–H stretching [41]; other peaks at 1310, 1314 and 1322 $cm^{-1}$ correspond to $\delta(CH_2)$ vibration and at 1451, 1456 and 1457 $cm^{-1}$ assignable to the $\delta(CH_3)$ vibrations [42]. Additional peaks at 894, 899, 1082, 1086, 1089 and 1094 $cm^{-1}$ can be attributed to $\nu$(CC) aliphatic chain vibrations [42].

## *2.2. Sample preparation*

Wan *et al.* [43] studied nanolubricants formulated with a commercial lubricating oil and h-BN nanoparticles with disk-like shape at different concentrations, concluding that 0.1 wt% in h-BN is the optimal concentration. Thus, this concentration was selected in the present work. On the other hand, a 1 wt% on IL has been selected based on the Zhou and Qu [11] and Bermúdez *et al.* [44] reviews and the results obtained by Otero *et al.* [31] of ILs as lubricant additives. Consequently, three mixtures were prepared: PAO 32 + 1 wt% IL1, PAO 32 + 1 wt% IL2 and PAO 32 + 1 wt% IL3, as well as the following dispersions: PAO 32 + 0.1 wt% h-BN, PAO 32 + 1 wt% IL1 + 0.1 wt% h-BN, PAO 32 + 1 wt% IL2 + 0.1 wt% h-BN and PAO 32 + 1 wt% IL3 + 0.1 wt% h-BN. The first dispersion was prepared using the two-step method. For the other three dispersions the following procedure proposed by Sanes *et al.* [21] was utilized. h-BN NPs were mixed with an IL in an agate mortar and stirred continuously for ten minutes. Then, the h-BN/IL sample was added to the PAO 32 oil. A high precision balance Sartorius MC 210P (0.00001 g precision) was used to determine the mass concentration of the h-BN NPs and the ILs. For homogenizing, the dispersions were sonicated in a Fisherbrand TM 11203 ultrasonic bath (frequency: 37 kHz, effective power: 180 W) for 4 hours continuously. Two sets of the mixtures

and dispersions were prepared, one to carry out the tribological investigations and the other to study the stability along time.

## *2.3. Thermophysical Characterization*

A SVM 3000 rotational Stabinger viscometer from Anton Paar (Graz, Austria) was used to measure the viscosities of PAO 32, the three PAO 32/IL mixtures and the four prepared nanodispersions from 278.15 to 373.15 K. The geometry of this viscometer is cylindrical with a rapidly rotating outer tube and an inner measuring bob that rotates more slowly. The relative expanded (k = 2) dynamic viscosity uncertainty is 1%. This apparatus also allows us to measure the density of the samples. The densimeter cell is a glass U-tube, which is excited to produce mechanical resonant vibrations according to DIN 51757 standard. The expanded uncertainties (k = 2) are 0.02 K for the temperature from 288.15 to 378.15 K and 0.05 K outside this range and 0.0005 $g \cdot cm^{-3}$ for density. More details of this equipment were reported previously [45, 46].

## *2.4. Tribological Tests*

The tribological tests for the neat lubricant (PAO 32), the three mixtures (PAO 32/IL), the nanolubricant (PAO 32/NPs) and the three hybrid nanolubricants (PAO 32/ILs/NPs), were carried out on a MCR 302 rheometer from Anton Paar (Graz, Austria), equipped with a Peltier heated tribology cell T-PTD200 in combination with a Peltier hood H-PTD 200 for precise temperature control, the configuration being ball-on-three-pins (Figure 3). The ball is fixed on a shaft, which is driven by the MCR rheometer motor. The three lower pins are inside a sample holder at a $45^{o}$ angle to the rotating shaft. In this configuration, during the test the ball rotates on the three pins under a fixed force, $F$, provided by the rheometer. This axial force, $F$, is transferred into three normal forces, $F_N$ acting perpendicular to the upper surface of the pins at the contact points, due to the ball pressing the three pins (see Figure 3) [47]. The flexibility of the bottom pins is required to get the same normal force acting evenly on all the three contact points of the upper ball. The rotating ball is adjusted automatically, and the forces are equally distributed on

208 the three friction contacts. From figure 3 it can be concluded that the relation between the
209 normal force $F_N$ acting on the three pins and the axial force $F$ exerted by rheometer is:

210 $$F_N = \frac{F}{3 \times \cos \alpha} \quad (1)$$

211 where α is the angle of the surface of the pins with the horizontal, which is 45º. From the torque
212 required to maintain the sliding speed, the frictional force, is obtained [48]. The software of the
213 tribological cell permits the selection of the value of either the axial force or the normal force.
214 More information on this equipment can be found in several articles [47-50].

215 The cylindrical pins of 6 mm height and the balls, both made of hardened 100Cr6 steel
216 and with a hardness of 62-66 Rockwell C, have diameters of 6 mm and 12.7 mm, respectively.
217 The roughness of the pins, Ra, was determined with a 3D Optical Profiler Sensofar (Terrassa,
218 Spain) S neox according to the standard ISO 4287, applying a Gaussian filter with a long
219 wavelength cut-off of 0.08 mm, being 0.09 μm. Hexane was used to clean the ball and the three
220 pins followed by a hot air drying before the test. In order to fully cover the top level of the pins,
221 1 ml of tested lubricant was added. The experiments were performed at 213 rpm rotational
222 speed (0.1 m $s^{-1}$) and 42.43 N axial load, *F*, distributed equally at the three pins (then each pin
223 supports a normal load of 20.00 N, Figure 3, which corresponds to a maximum Hertzian pressure
224 of 1.05 GPa) for 3400 seconds at 298.15 K and 353.15 K. Three trials were performed for each
225 friction test to obtain accurate experimental average values. After these tests, the pins were
226 cleaned in a hexane ultrasonic bath for one minute to remove the residual lubricant in the wear
227 scar. Wear (diameter, area, depth and volume) on the worn surface of the three pins was
228 measured by means of the 3D optical profilometer (Sensofar S neox), working in confocal mode
229 using a 10x objective and the SensoMAP software, integrated with the profiler, which provides
230 fast and accurate analysis of surface geometry with tools for measuring distances, areas of peaks
231 and valleys or volumes of holes, among others. As regards worn area measurements, firstly, a
232 cross section profile of worn surface is generated by the 3D profiler and then the software
233 determines the area as the subtraction of the worn area minus the sum of the areas of the

profiles of the material displaced on both sides of the worn track. The wear volume is measured inputting the level of the unworn surface of the pin using the hole perimeter at this level. The software then automatically determines the coordinates of the profile points of the wear surface and calculates the hole volume below this level. SEM analyses were conducted with a Carl Zeiss FESEM ULTRA Plus Scanning Electron Microscope on the worn surface to examine its morphology. In addition, to obtain information about the composition in the wear track, a WITec alpha300R+ confocal Raman microscopy was used.

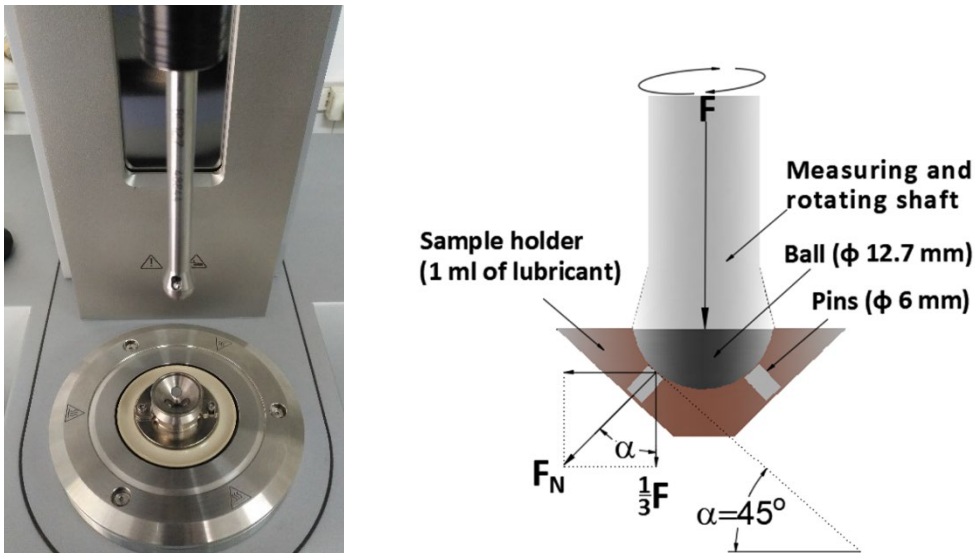


**Fig. 3.** Picture and 2D drawing of the tribometer test setup

## 3. Results and discussion

### *3.1. Stability of the mixtures and nanodispersions*

Visual observation was the method used to analyze the stability of the ILs and the NPs in PAO 32 base oil. The previously prepared samples were kept and preserved at room temperature with no disturbance. Successively, the samples were observed daily to detect any sedimentation at the bottom of the container. The photographs taken are shown in Figure 4 for PAO 32/IL mixtures and Figure 5 for the nanolubricants. As can be seen in Figure 4, for the three PAO 32 + IL systems, no signs of immiscibility were detected for 240 days after the preparation of the mixture.

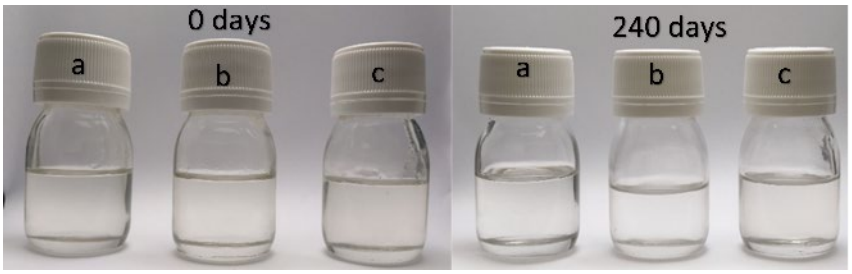


252

253 **Fig. 4.** Photographs used for checking the stability of the mixtures: (a) PAO 32 + 1 wt% IL1, (b)
254 PAO 32 + 1 wt% IL2, (c) PAO 32 + 1 wt% IL3.

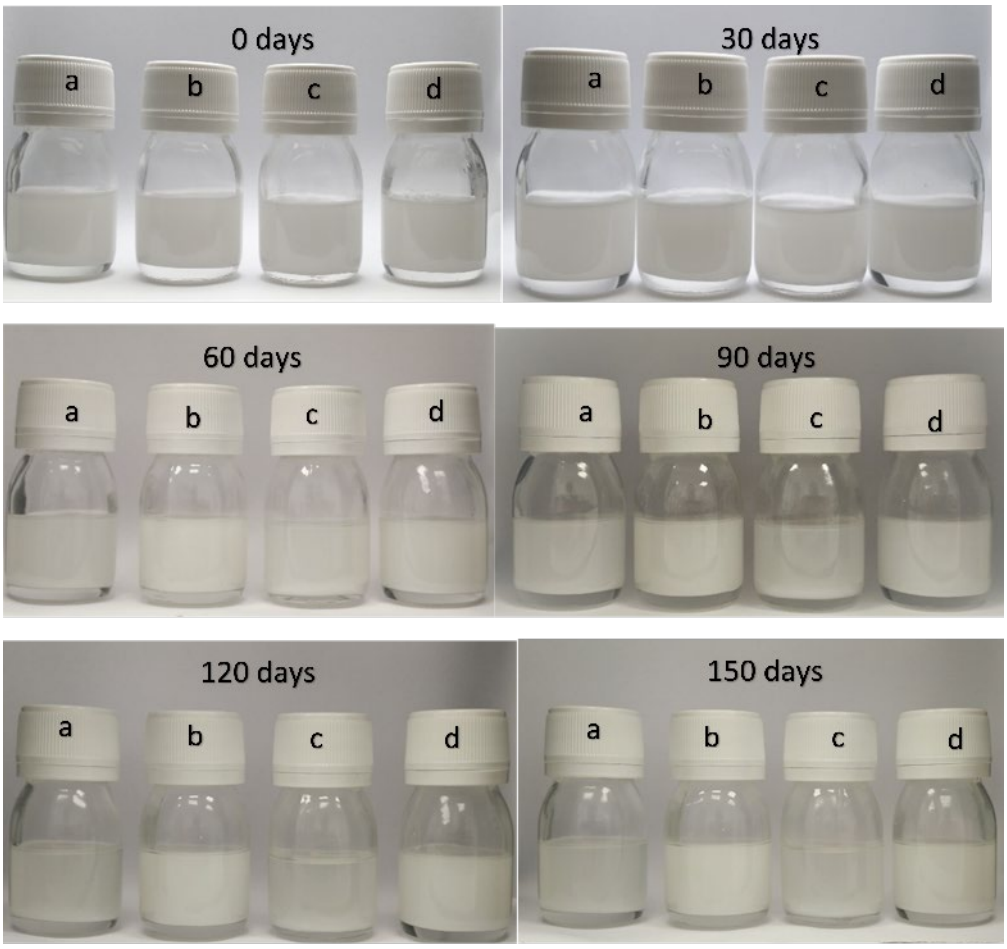


255

256 **Fig. 5.** Photographs used for assigning the stability of the nanodispersions: (a) PAO 32 + 0.1
257 wt% h-BN, (b) PAO 32 + 1 wt% IL1 + 0.1 wt% h-BN, (c) PAO 32 + 1 wt% IL2 + 0.1 wt% h-BN, (d)
258 PAO 32 + 1 wt% IL3 + 0.1 wt% h-BN.

259

260 Figure 5 clearly shows that the presence of ILs improves the temporal stability of the
261 nanodispersions. Thus, the PAO 32/h-BN nanodispersion presents partial sedimentation
262 between the thirtieth and sixtieth day after preparation, whereas the PAO 32/IL2/h-BN
263 nanodispersion shows partial instability between 60 and 90 days and the other nanodispersions

remain stable till 150 days. It can also be concluded that the individual use of ILs as additives to the oil leads to longer stability compared to those obtained with h-BN as singular additive or with ILs combined with NPs as hybrid additives as well. Finally, photos were taken after 240 days from preparation (Figure S3), indicating that the ionic liquids that keep h-BN NPs dispersed in PAO 32 for longer are those based on ILs the cations with longer alkyl chains ($[P_{6,6,6,14}]^+$), IL1 and IL3.

In addition, FTIR spectra have been recorded for the mixtures and nanodispersions analyzed, comparing these spectra with the one corresponding to PAO 32. As can be observed from Figure S4, no significant changes were found, therefore it seems that no new chemical bonds are formed in the dispersions and the mixtures.

## *3.2. Thermophysical Characterization*

The dynamic viscosity ($\eta$) and the density ($\rho$) at atmospheric pressure of the PAO 32 base oil and the prepared samples with different additives at temperatures from 278.15 K to 373.15 K are reported in Tables S1 and S2. Density values of the dispersions and the mixtures are slightly higher than those of PAO 32, the increase in the density of the base oil due to the addition of h-BN nanoparticles or/and ILs ranges from 0.06 % to 0.30 %. The average increase in density over the whole temperature range is plotted in Figure S5.

Viscosity values of the dispersions and the mixtures are higher than those of PAO 32. The viscosity of the base oil increases due to the addition of h-BN nanoparticles or/and ILs up to 7.0 %. The average increase in viscosity over the whole temperature range is plotted in Figure S6. The highest average relative dynamic viscosity is reached for the nanodispersion PAO 32/IL2/h-BN followed by the PAO 32/IL2 mixture. It was also found that the viscosity temperature dependence of the mixtures and nanodispersions are similar to that of PAO 32.

## *3.3. Corrosion test*

Corrosion tests of the ILs were carried out on smooth surfaces of 100Cr6-steel disks of 10 mm diameter and 190-210 Hv30 hardness. The disks were cleaned using an ultrasonic technique

290 in a hexane bath for five minutes, rinsed with a stream of ethanol and then dried with hot air.
291 Three drops (around 0.15 ml) of IL1, IL2, or IL3 were applied on the surface of the disks as shown
292 in Figure 6. Finally, these disks were placed inside Petri dishes with lids for 35 days in room
293 conditions. It was observed that the surface of the disk with IL2 rapidly showed corrosion within
294 a day of its application whereas for the disks with IL1 and IL3 no corrosion was detected neither
295 after one day nor after 35 days. To confirm these results, surface roughness, Ra, was measured
296 on the covered area. Obtained Ra values are plotted in Figure 7 where the surfaces of the unused
297 disk and those of the disks wet with IL1 and IL3 have the same Ra value (0.0076 μm) whereas
298 the surface wet with IL2 exhibits a higher Ra value (0.061 μm).
299

| Time(hours) | IL1 | IL2 | IL3 |
|---|---|---|---|
| Just after preparation |  |  |  |
| One day after preparation |  |  |  |
| 35 days after preparation |  |  |  |
| Just after being kept in a chamber for 24 hours at 373 K |  |  |  |

300 **Fig. 6.** Photographs of the disks during corrosion tests

Three other disks with ILs were prepared and kept in a temperature chamber at 373.15 K for 24 hours, to analyze the effect of the water contained in the ILs. The temperature was kept constant within 0.3 K inside this chamber. After this period, the photos shown in Figure 6 were taken. In this case, no corrosion was detected in the three disks. Hence in the ambient tests the corrosion of the IL2 disk is due to the presence of water.

In addition, the used ILs in this test were analyzed by infrared spectroscopy (Figure S7). As can be observed, while the fresh IL samples did not show the typical peaks of water [40], the used ILs in corrosion tests at room conditions and even those used at 373.15 K present these peaks. Hence, in contact with air, the three ILs are quickly hydrated.

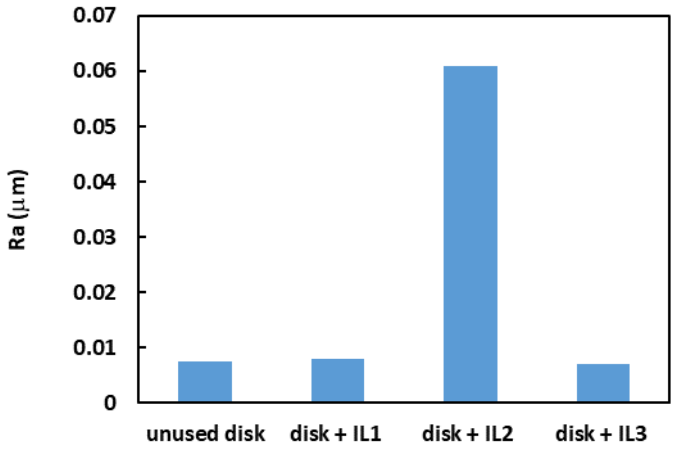


**Fig. 7.** Roughness values (Ra) of the surfaces for unused and wet disks by different ionic liquids (Gaussian filter 0.08 mm)

## *3.4. Lubrication performance and friction behavior*

Figure 8 shows friction coefficients evolution along time for PAO 32, the three PAO 32 + ILs mixtures, the PAO 32 + h-BN and the three PAO 32 + ILs + h-BN dispersions at 298.15 K and 353.15 K. As expected, the fluctuations and the friction values at 353.15 K are higher than those at 298.15 K. Central specific film thickness, λ, has been calculated for all the dispersions and mixtures at 298.15 K and 353.15 K using the Hamrock-Dowson model [51, 52]. As a result of the

viscosity decrease when temperature rises, central film thickness diminishes, thus at 298.15 K it is close to 209-217 nm (λ= 1.47-1.54) whereas at 353.15 K it is around 32.0-33.2 nm (λ= 0.226-0.234). Consequently, friction is more severe and presents more time fluctuations at 353.15 K because more asperities are in contact. Figure 9 and Table 2 show, for each lubricant, the average friction coefficients of the three replicates for the whole test time of each test. All the additives improved base oil friction behavior, especially at 353.15 K. Friction reductions range from 7 % to 17 % at 298.15 K, whereas at 353.15 K vary from 2 % to 28 %. The reductions due to h-BN are the lowest, being 2 % and 7 % at 353.15 K and 298.15 K, respectively. Regarding PAO32 + ILs, at 298.15 K, IL1 ($[P_{6,6,6,14}][DEHP]$) showed the best reduction being 12 %, whereas at 353.15 K, a maximum reduction of 25 % was obtained with IL2 ($[P_{2,4,4,4}][DEP]$) as additive. In the case of nanolubricants, for both temperatures the lowest friction coefficients were obtained for PAO 32 + IL2 + h-BN, 28 % reduction at 353.15 K and 17 % reduction at 298.15 K, being the lowest anti friction capabilities, 12 % reduction at 353.15 K and 7 % reduction at 298.15 K, for PAO 32 + IL3 + h-BN.

**Table 2.** Mean average values of the friction coefficient (μ), its % reduction and the corresponding standard deviation (σ) for all lubricants at 298.15 K and 353.15 K

| | 298.15 K | | | 353.15 K | | |
|---|---|---|---|---|---|---|
| Lubricant | μ | σ | % friction reduction | μ | σ | % friction reduction |
| PAO 32 | 0.088 | 0.0017 | - | 0.115 | 0.0010 | - |
| PAO 32 + 1 wt% IL1 | 0.081 | 0.0003 | 12 | 0.096 | 0.0032 | 16 |
| PAO 32 + 1 wt% IL2 | 0.087 | 0.0029 | 6 | 0.085 | 0.0043 | 25 |
| PAO 32 + 1 wt% IL3 | 0.086 | 0.0013 | 7 | 0.114 | 0.0030 | 2 |
| PAO 32 + 0.1 wt% h-BN | 0.086 | 0.0023 | 7 | 0.113 | 0.0014 | 2 |
| PAO 32 + 1 wt% IL1+ 0.1 wt% h-BN | 0.083 | 0.0005 | 10 | 0.100 | 0.0024 | 13 |
| PAO 32 + 1 wt% IL2+ 0.1 wt% h-BN | 0.077 | 0.0021 | 17 | 0.083 | 0.0046 | 28 |
| PAO 32 + 1 wt% IL3+ 0.1 wt% h-BN | 0.086 | 0.0034 | 7 | 0.101 | 0.0096 | 12 |

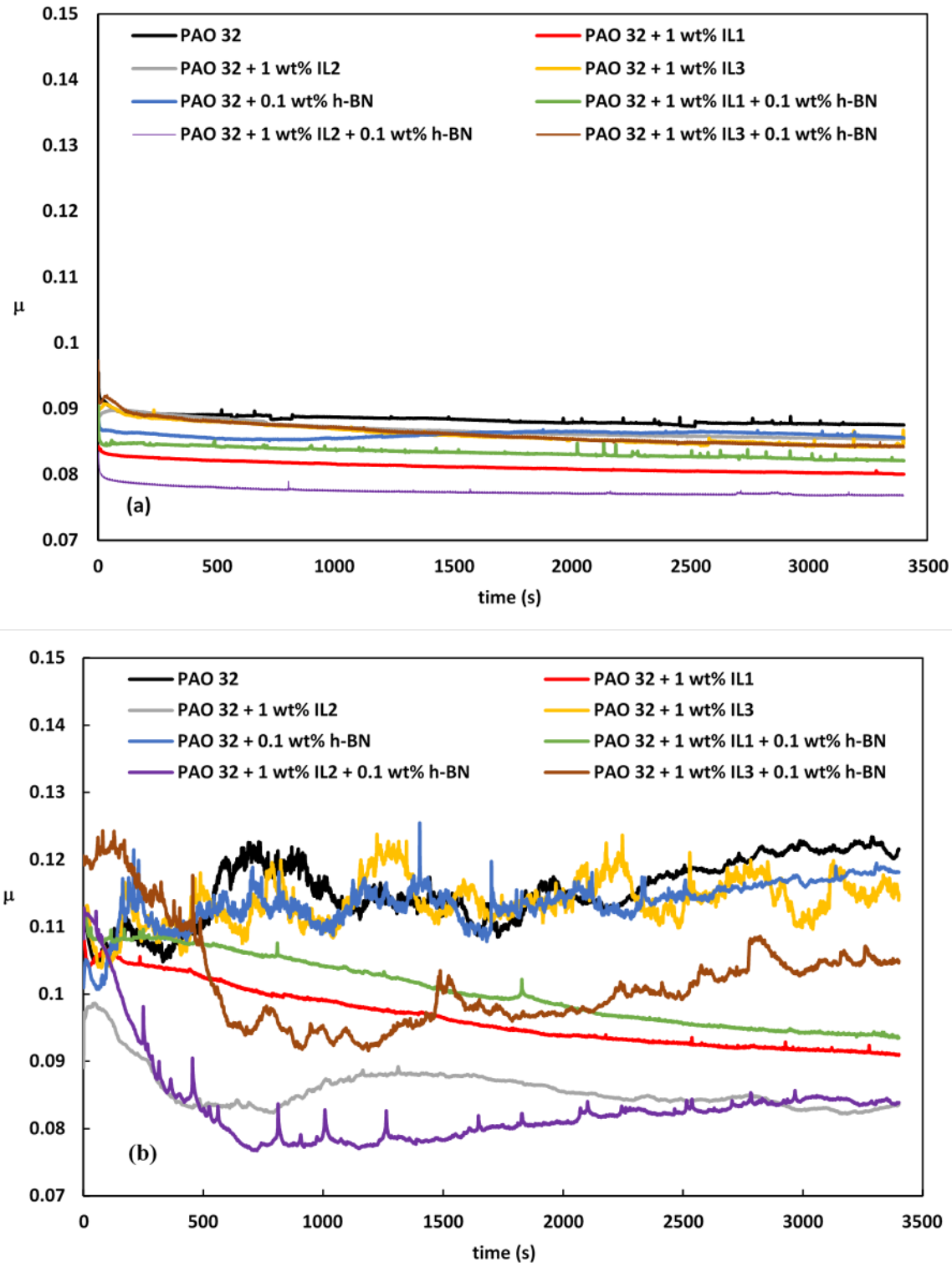


337

338 **Fig. 8.** Coefficient of friction (μ) of the different samples along time (s): (a) at T= 298.15 K and

339 (b) at T= 353.15 K

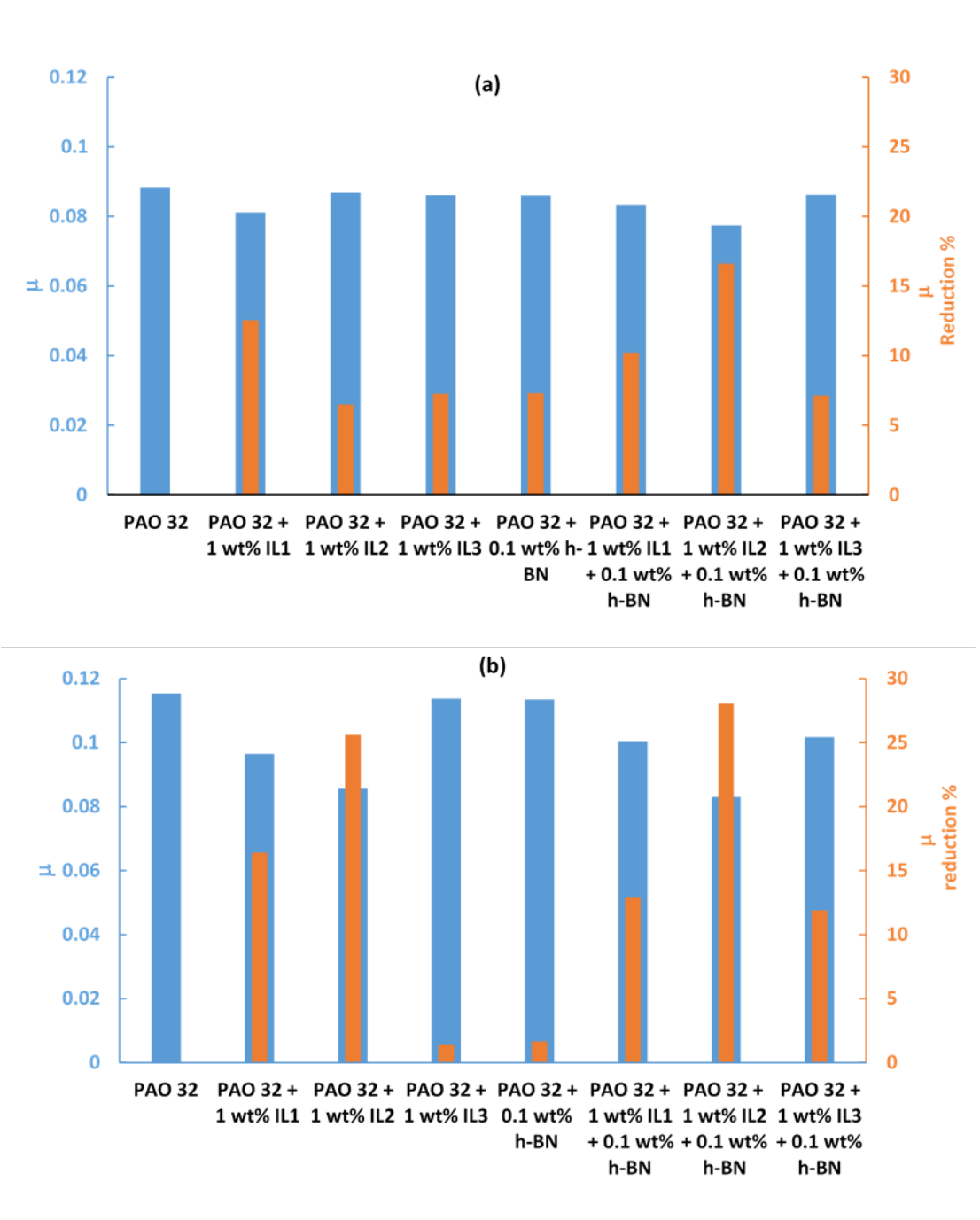


**Fig. 9.** Average coefficient of friction (μ) and its reduction using the different lubricants compared with the PAO 32 base oil: (a) at T= 298.15 K and (b) at T= 353.15 K

### *3.5. Surface analysis and wear behavior*

Figure 10 shows the images obtained with the optical profilometer of the wear scar at the pins tested with PAO 32 at 298.15 K and 353.15 K. It shows the wear scar clearly identified at

346 the higher temperature, being unmeasurable at 298.15 K. For this reason, it was not possible to
347 determine the diameter (WSD), the cross-section area and the deepness of the wear scar. In
348 Table 3 the average values at 353.15 K of the wear parameters are given. Three track profiles
349 were taken in three different sections of the wear track in the pins, and the different wear
350 parameters measured. Then the values reported in Table 3 are the corresponding mean values.
351

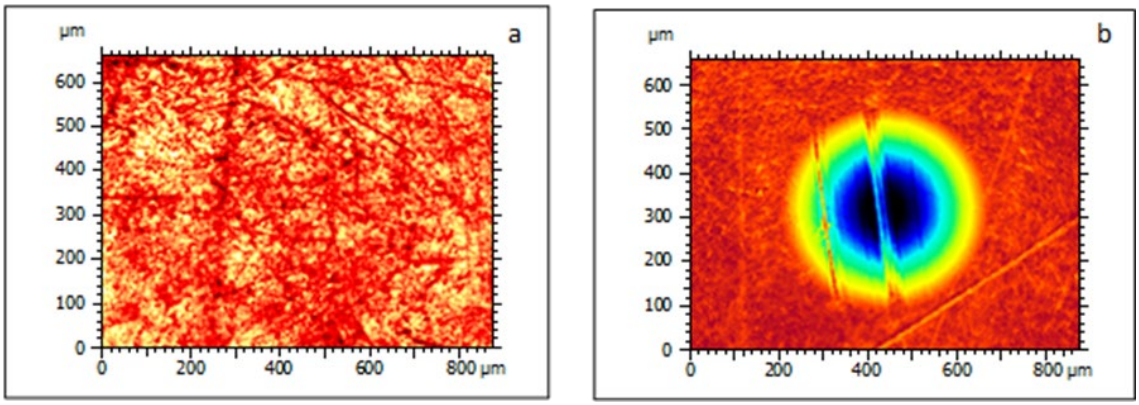


352

353 **Fig. 10.** 2D-Optical micrograph (10x) of the wear track at the pin surface lubricated by PAO 32:
354 (a) at T= 298.15 K and (b) at T= 353.15 K

355

356 According to Table 3 and Figure 11 at 353.15 K, the WSD of the neat PAO 32 was the
357 highest, recording 465 µm, followed by a close value of 445 µm when 0.1 wt% of h-BN was
358 dispersed in the lubricant. The rest of the mixtures and dispersions showed better anti wear
359 abilities, thus the addition of IL1, IL2 or IL3 separately lead to 50, 48 and 22 % WSD reduction
360 compared to the performance of the PAO 32. The hybrid combination of IL1 ($[P_{6,6,6,14}][DEHP]$)
361 and h-BN resulted in a more significant reduction of WSD which was 65 %. SEM images of the
362 wear scars on the pins were taken with the Carl Zeiss FESEM ULTRA Plus SEM. As seen in Figure
363 12, the SEM images agree with the results obtained for WSD with the profilometer. Thus, the
364 image order in Figure 12 reflects the trend of the wear scar size.

365

366 **Table 3.** Mean average values of the friction coefficient (μ), the wear scar diameter (WSD), the cross-section area, the volume of the wear and the

367 maximum wear depth of the wear track with their % reduction and the corresponding standard deviation, σ, for all lubricants at 353.15 K

368

| Lubricant | WSD/ μm | σ/μm | % diameter reduction | Area/ $\mu m^2$ | σ/$\mu m^2$ | % Area reduction | Volume/ $\mu m^3$ | σ | % volume reduction | depth/ μm | σ/μm | % depth reduction |
|---|---|---|---|---|---|---|---|---|---|---|---|---|
| PAO 32 | 465 | 5.0 | - | 992 | 10 | - | 166952 | 01394 | - | 3.41 | 0.015 | - |
| PAO 32 + 1 wt% IL1 | 230 | 2.0 | 50 | 180 | 05 | 82 | 5683 | 00024 | 97 | 0.52 | 0.011 | 85 |
| PAO 32 + 1 wt% IL2 | 240 | 2.0 | 48 | 190 | 08 | 80 | 32042 | 00036 | 80 | 1.93 | 0.011 | 44 |
| PAO 32 + 1 wt% IL3 | 360 | 2.5 | 22 | 588 | 10 | 41 | 80656 | 00079 | 52 | 3.00 | 0.010 | 11 |
| PAO 32 + 0.1 wt% h-BN | 445 | 5.4 | 5 | 947 | 10 | 4 | 158857 | 00434 | 5 | 3.31 | 0.017 | 2 |
| PAO 32 + 1 wt% IL1+ 0.1 wt% h-BN | 165 | 5.3 | 65 | 29 | 05 | 97 | 1269 | 00025 | 99 | 0.28 | 0.015 | 92 |
| PAO 32 + 1 wt% IL2+ 0.1 wt% h-BN | 299 | 2.5 | 35 | 174 | 08 | 82 | 12565 | 00048 | 92 | 0.94 | 0.014 | 73 |
| PAO 32 + 1 wt% IL3+ 0.1 wt% h-BN | 291 | 4.0 | 37 | 195 | 03 | 80 | 24245 | 00036 | 85 | 1.32 | 0.011 | 61 |

369
370

From Table 3 it can be also concluded that the cross-section area and the wear volume were reduced with all the additives. The area and volume reductions range respectively from 4 % and 5 % for PAO 32 + 0.1 wt% h-BN to 97 % and 99 % for PAO 32 + 1 wt% IL1+ 0.1 wt% h-BN. A similar trend was found for the depth reduction, in this case ranging from 2 % to 92 % for the same dispersions (Table 3). For a better comparison, Figure 13 shows all the transversal profiles of the different scars. As can be observed, the best anti-wear results were found for both the mixture and the nanodispersion containing IL1 ([$P_{6,6,6,14}$][DEHP]).

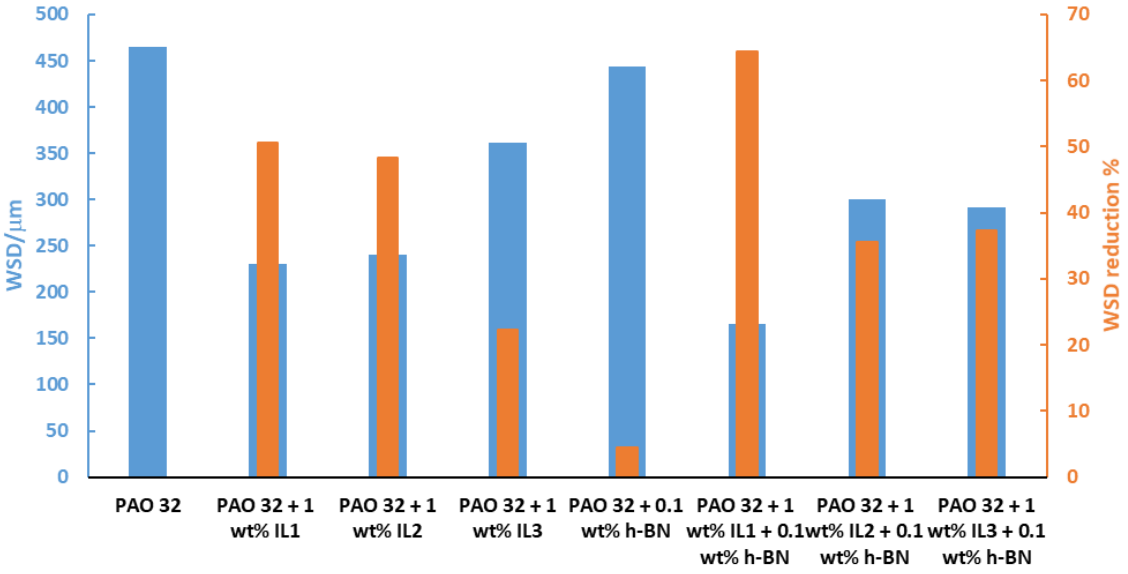


**Fig. 11.** Wear scar diameter (μm) at the surface of the steel pins using different lubricants, and its reduction (%) compared with PAO 32 base oil performance at T= 353.15 K

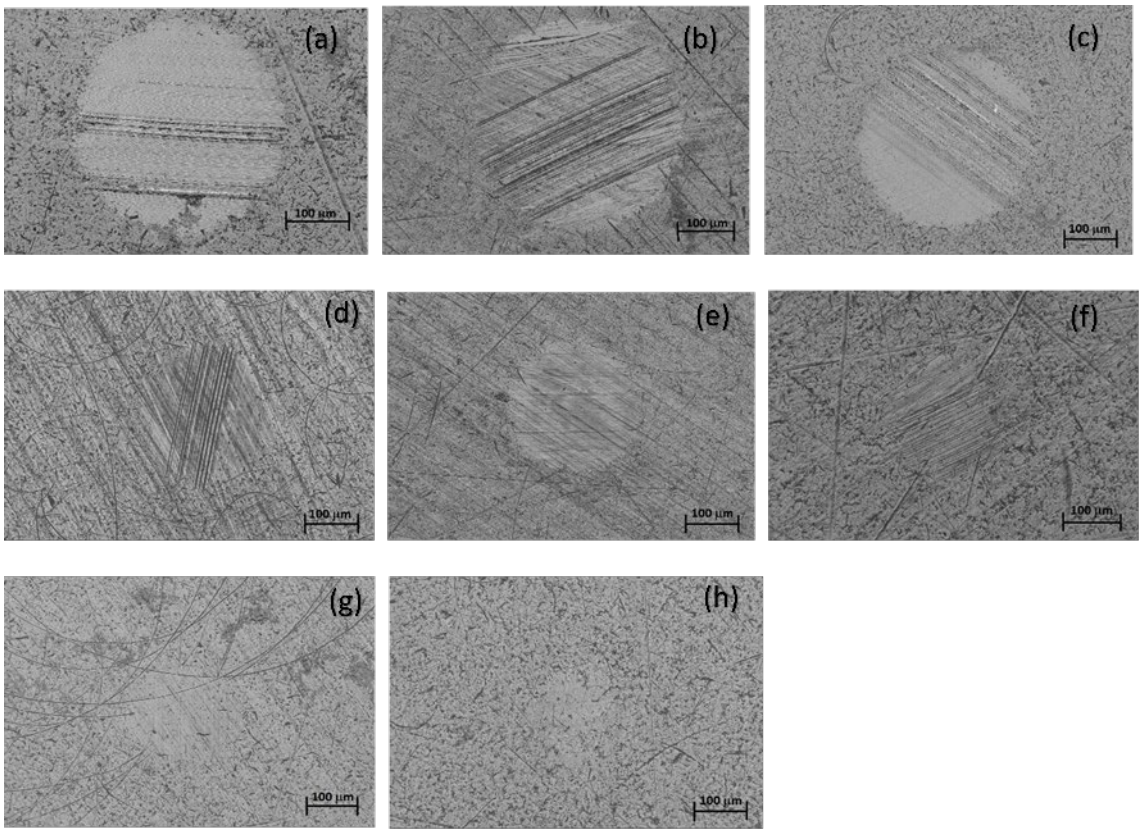


382

383 **Fig. 12**. SEM images of the wear scars at the surface of the pins lubricated by: (a) PAO 32, (b)

384 PAO 32 + 0.1 wt% h-BN, (c) PAO 32 + 1 wt% IL3, (d), PAO 32 + 1 wt% IL2 + 0.1 wt% h-BN (e), PAO

385 32 + 1 wt% IL3 + 0.1 wt% h-BN (f) PAO 32 + 1 wt% IL2, (g) PAO 32 + 1 wt% IL1 and (h) PAO 32 +

386 1 wt% IL1 + 0.1 wt% h-BN at 353.15 K and a scale of 100 μm. The images are ordered from higher

387 to lower wear.

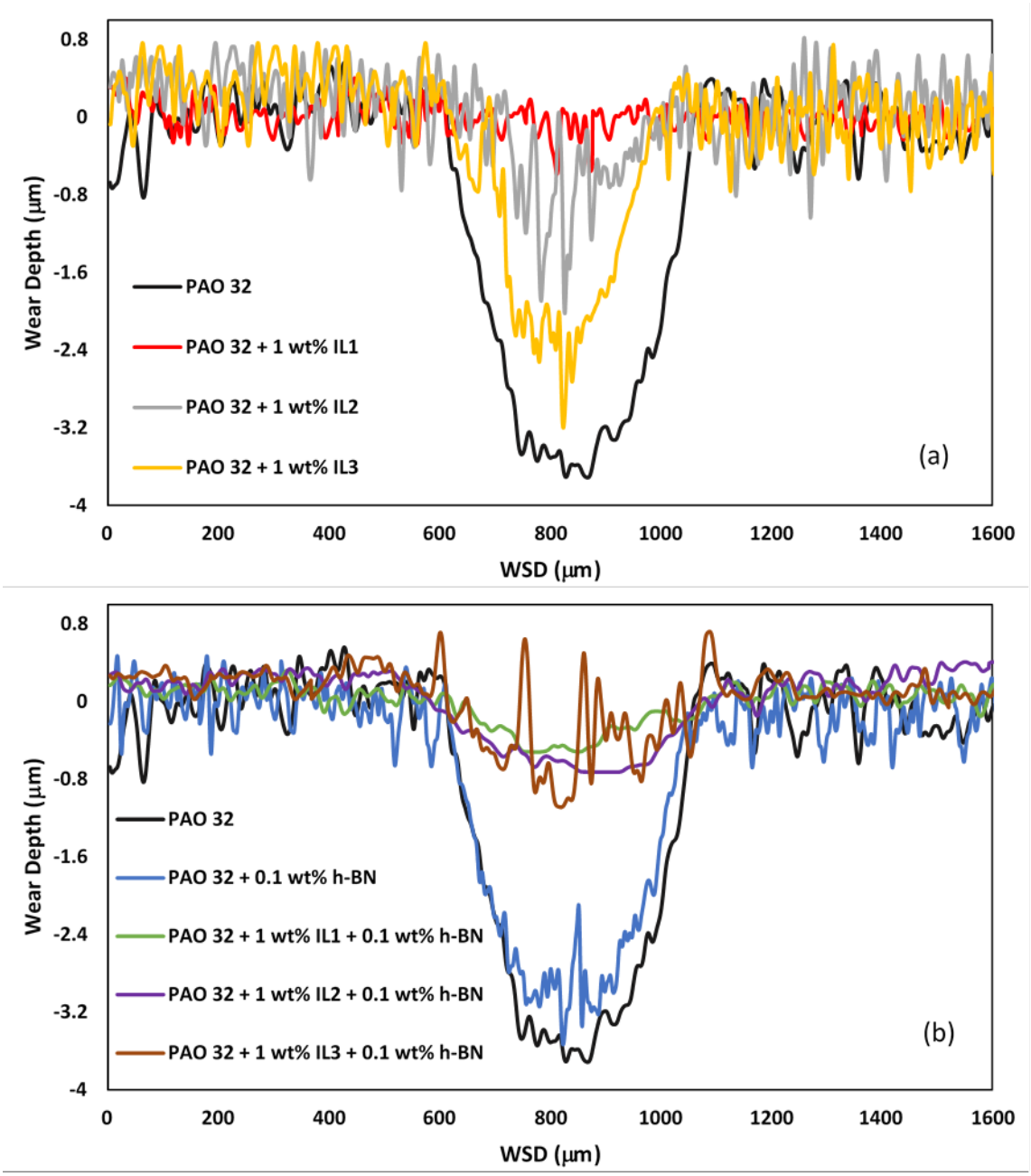


388

389 **Fig. 13.** Wear track profile at the surfaces of the pins lubricated by the mixtures at T= 353.15 K:
390 (a) for PAO 32, PAO 32 + 1 wt% IL1, PAO 32 + 1 wt% IL2 and PAO 32 + 1 wt% IL3, and (b) for PAO
391 32, PAO 32 + 0.1 wt% h-BN, PAO 32 + 1 wt% IL1 + 0.1 wt% h-BN, PAO 32 + 1 wt% IL2 + 0.1 wt%
392 h-BN and PAO 32 + 1 wt% IL3 + 0.1 wt% h-BN

393

394 Figure 14 shows the roughness (Ra) of the scar surfaces of the pins lubricated with
395 different lubricants at 353.15 K measured according to the standard ISO 4287 with the 3D

Optical Profiler, applying a Gaussian filter with a long wavelength cut-off of 0.08 mm. The highest reduction of the Ra was achieved by the addition of IL2 and h-BN to PAO 32 being 0.02 μm leading to a reduction of 60 % compared to that of the untested surface which is 0.09 μm. Moreover, the hybrid combination of h-BN and IL1 or IL3 added to PAO 32 leads to Ra values of 0.04 μm and 0.05 μm respectively. It is interesting to note that the roughness of the surfaces lubricated with the three ILs mixtures roughly decreases the value corresponding to PAO 32 whereas for the surface lubricated with the nanodispersion PAO 32 + 0.1 wt% h-BN a higher Ra value was obtained. Hence, and regarding smoothness or the worn surface, positive synergies were found for h-BN and each one of the three ILs.

Hybrid additive IL1 ($[P_{6,6,6,14}][DEHP]$) and h-BN leads to the highest antiwear capability of all the tested PAO 32 lubricants whereas hybrid additive $[P_{2,4,4,4}][DEP]$)/h-BN leads to a better antifriction performance and to the smoothness surface of all the tested PAO 32 lubricants.

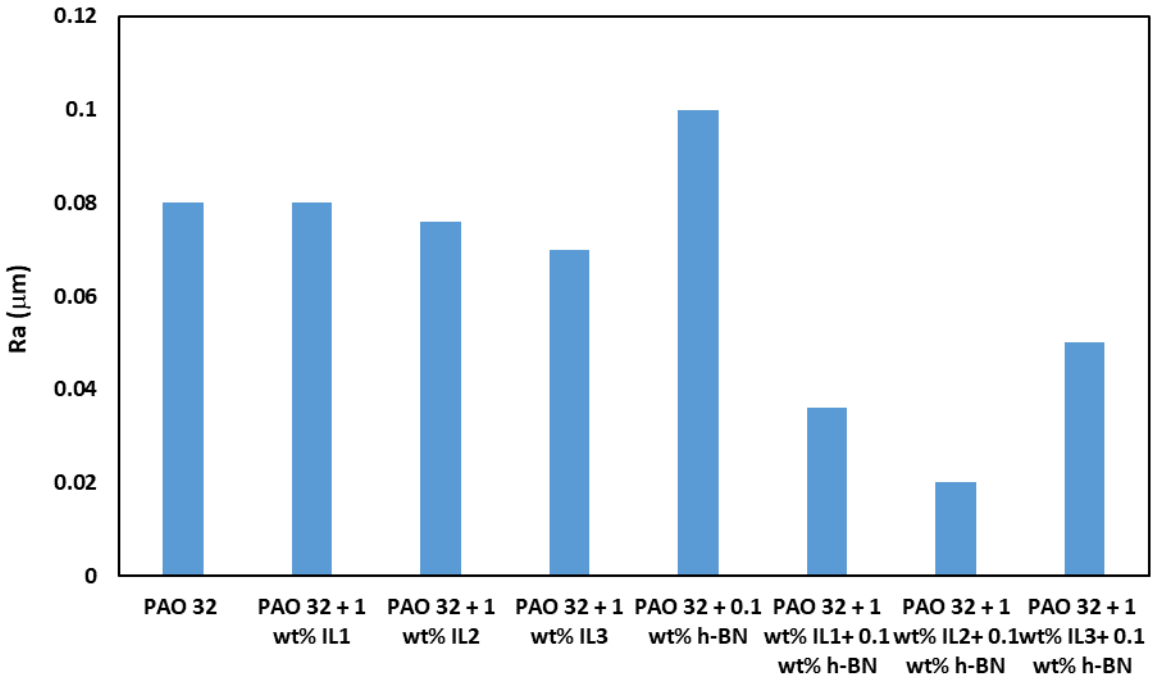


**Fig. 14.** Average Roughness value (Ra) at the contact surface of the steel pins lubricated with the different mixtures at T= 353.15 K

Raman spectra on the worn surfaces tested at 353.15 K were performed with a WITec alpha300R+ confocal Raman microscopy at a wavelength of 532 nm. Accordingly, Figure 15 and Figures S8-S13 show the results obtained for the pins lubricated with PAO 32, PAO 32 + 1 wt% IL, PAO 32 + 0.1 wt% h-BN and the nanodispersions PAO 32 + 1 wt% IL+ 0.1 wt% h-BN at 353.15 K. Due to the close spectrum shape of PAO 32 and the ILs, the most dissimilar peaks were identified to differentiate between the PAO 32 and the ILs present at the worn surface. The Raman spectra of PAO32 is shown in Figure S1 indicting the highest peak of 2857 $cm^{-1}$, Figure S2 shows the highest peaks of the three ILs to be 2908 $cm^{-1}$ for IL1, 2930 $cm^{-1}$ for IL2 and 2909 $cm^{-1}$ for IL3. As indicated in Figure 15 (a and b) the peak 2857 $cm^{-1}$ corresponds to PAO 32 whereas the peak at 2907 $cm^{-1}$ corresponds to IL1. Figures S8 to S13 show the Raman of the rest of the surfaces and the corresponding peaks are indicated to identify the exact materials present at the worn surface.

All figures show the mapping of the compounds found in the worn surfaces. In all cases the mappings indicate that adsorbed films were formed on the rubbing surfaces, and show areas where the spectrum coincides with that of PAO 32 as well as other areas corresponding to the carbon spectrum, may be due to the carbonization of the lubricant base owing to the local high temperature during the sliding [53] or during the Raman spectrum tests.

As regards the worn surfaces lubricated with the three PAO 32 + 1 wt% IL mixtures as shown in Figures S8-S10, the areas corresponding to the PAO32 are similar, those corresponding to the ILs follow the trend IL1≈IL2< IL3 and for the iron oxide areas the trend is IL1<IL2≈IL3. IL1 and IL2 show excellent behavior as additives at boundary conditions because they are present in the worn surface in a slightly larger proportion than the IL concentration of the mixtures. IL1 ($[P_{6,6,6,14}][DEHP]$) presents the best antifriction behavior at 298.15 K and the best antiwear capability at 353.15 K. According to Kawada et al. [54] the lubricity of the IL is determined by the structure of the anion. Hence $[DEHP]^-$ anion displays good antiwear and antifriction properties.

438 The worn surfaces lubricated with the three PAO 32 + 1 wt% IL+ 0.1 wt% h-BN
439 nanodispersions also present important areas corresponding to the ionic liquids (pink) following
440 the same trend as the PAO 32 + 1 wt% IL mixtures. Regarding the presence of h-BN (yellow) on
441 the worn surfaces lubricated with the four nanodispersions shown in Figures S11-13 and Figure
442 15 b, the area trend is PAO32+IL1+h-BN<PAO32+IL2+h-BN≈PAO32+IL3+h-BN<PAO32+h-BN. The
443 presence of h-BN in the worn surfaces lubricated with all the nanodispersions is scarce, likely
444 due to the small concentration (0.1 wt%). It should be pointed out that the nanodispersion PAO
445 32 +h-BN roughly improves the tribological performance of PAO 32, and leads to the roughest
446 surface, presenting clear signs of abrasive wear (Figure 12b). In addition, the tribofilms formed
447 by PAO 32 + IL1 +h-BN are more effective in protecting the steel surface because a lower
448 presence of both additives leads to the better antiwear capability than with the other two
449 nanolubricants containing IL2 or IL3. Nevertheless, the nanolubricants containing IL2 or IL3 and
450 h-BN present, with the only exception of WSD, better antiwear performances than the
451 corresponding PAO 32 + IL mixtures. Thus, this fact proves the positive synergies between both
452 types of additives.

453 Taking into account that in the boundary lubrication regime it is more interesting to
454 reduce wear than friction because wear can directly cause the breakdown of the mechanical
455 components [55], PAO 32 + IL1 + h-BN is the nanolubricant that displays the best tribological
456 performance of those studied in this work.

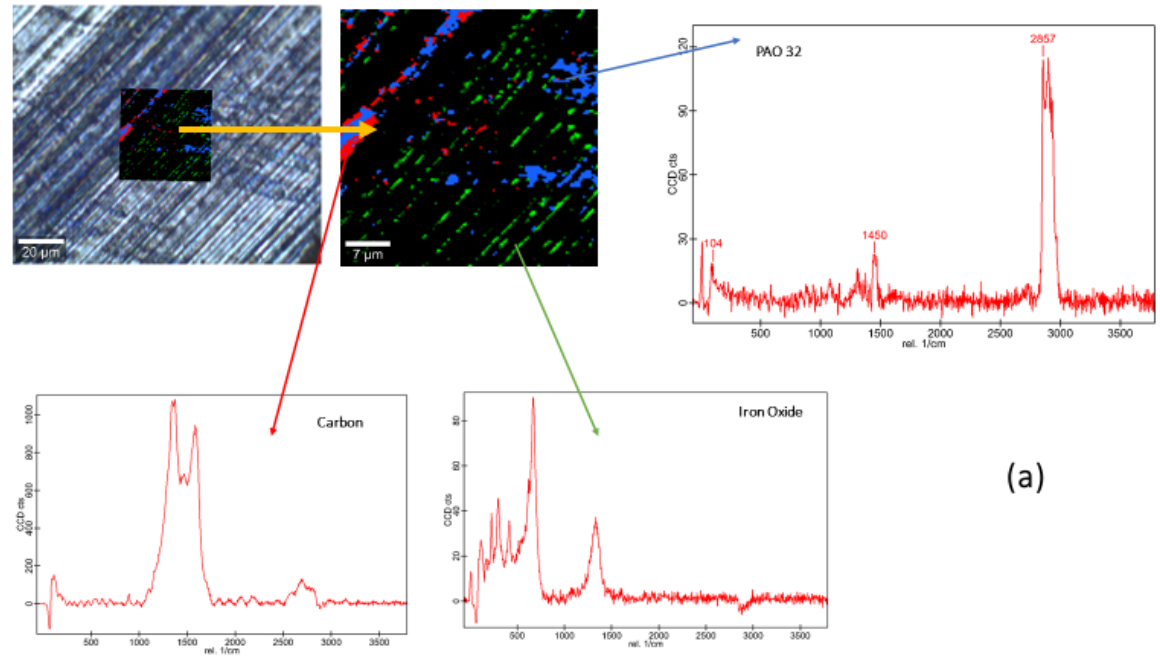


457

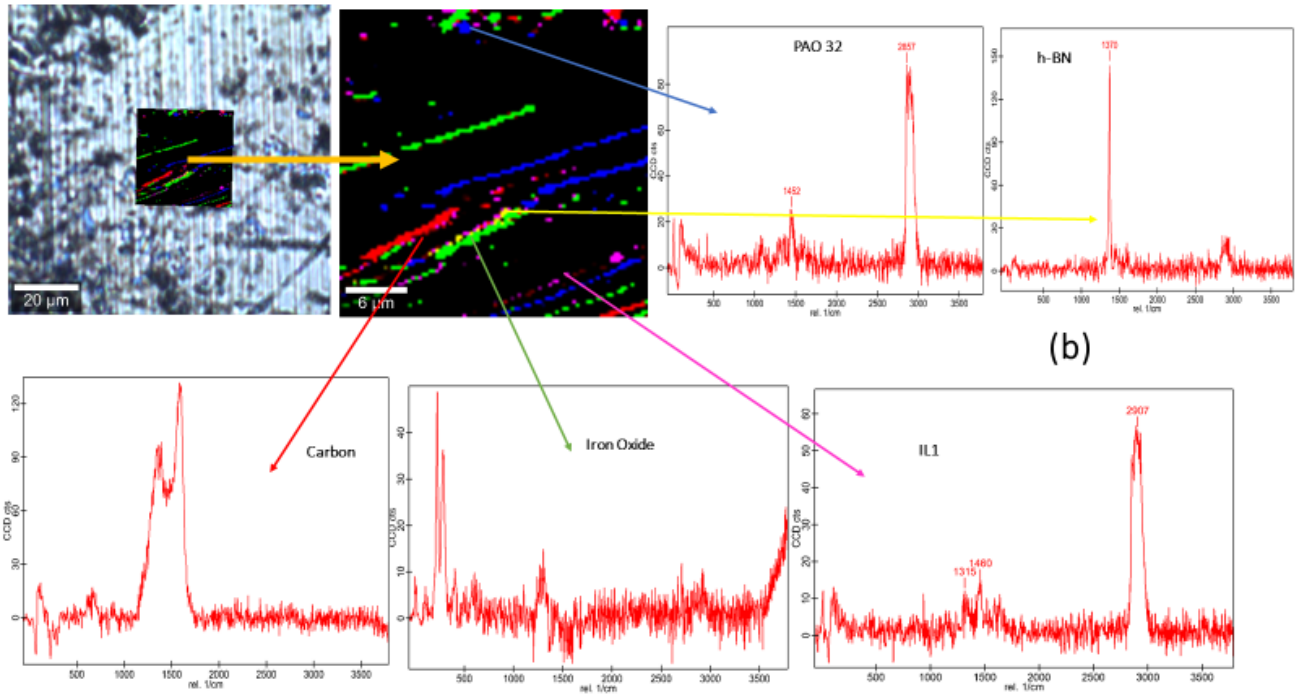


458

459 **Fig. 15**. Raman spectra and element map combination at the worn surface lubricated by: (a)

460 PAO 32 and (b): PAO 32 + 1 wt% IL1+ 0.1 wt% h-BN at 353.15 K

461

462 With regards to oxide formation, we have additionally performed Raman analyses out

463 of the wear scar on the pins. No signs of oxide formation were found in any of the specimens

lubricated with the lubricants tested. Consequently, their presence is due to the tribological process itself. Recently, Ratoi et al. [56] investigated the tribological performance of PAO 32 as lubricant to a 100Cr6/100Cr6 steel contact pair in different atmospheres (air, hydrogen and argon) at 393.15 K. These authors have carried out X-ray photoelectron spectroscopy (XPS) analyses on the wear track in order to investigate the nature of the tribofilm formed during the tests. It is interesting to note that iron oxides were detected in all the cases, in fact those tribofilms are mainly formed by carbon, iron and oxygen [56]. These authors concluded that, among other effects, the build-up of a tribofilm through oxide formation and lubricant degradation on the wear track led to smoother wear.

In the tribological tests performed in this work, a tribopair steel/steel was used. These steel surfaces are more reactive counterfaces than other metallic alloys, so promote the decomposition of the IL due to the reaction with iron [44]. For the three ILs tested as additives in this work, both anion and cation contain phosphorous, therefore it is difficult to determine if tribofilms are due to the decomposition of the cation, the anion or both [57]. In addition, due to the positive charge induced by tribo-stress, anions tend to be adsorbed on the steel surface, thus control the lubricity of the IL [24]. The three ILs reduce the friction and wear, being the lowest reductions (mainly at 353.15 K) for $[P_{6,6,6,14}][(iC_8)_2PO_2]$. Cowie et al. [58] found that $[P_{6,6,6,14}]$[DEHP] when mixed with hexadecane, is more effective than $[P_{6,6,6,14}][(iC_8)_2PO_2]$ in AFM nanotribology and alumina surfaces. These authors suggest that the former is adsorbed more effectively in charged alumina surface creating a smoother and more robust ion boundary layer, since the electrical conductivity of $[P_{6,6,6,14}]$[DEHP]/oil mixture is about 2 orders of magnitude higher than that of $[P_{6,6,6,14}][(iC_8)_2PO_2]$/oil mixture at the same concentration [59]. This means that $[P_{6,6,6,14}]$[DEHP] dissociates more to single ions when dissolved in apolar oils than $[P_{6,6,6,14}][(iC_8)_2PO_2]$.

As regards results concerning friction, hybrid additive $[P_{2,4,4,4}]$[DEP]/h-BN leads to a better antifriction performance and to a smoother worn surface of all the tested PAO 32

lubricants, which could indicate that ILs containing anions with linear alkyl chains display a better antifriction behavior than those with anions with ramified alkyl chains. On the other hand, hybrid additive $[P_{6,6,6,14}][DEHP]$/h-BN leads to the highest antiwear capability of all the tested PAO 32 lubricants, whereas the corresponding to $[P_{6,6,6,14}][(iC_8)_2PO_2]$ the lowest, in agreement with the results obtained with PAO32/IL mixtures. These results seem to indicate that the antiwear capability is more influenced by the anion of the IL than by the cation. In addition, high branching in the anion alkyl chains could have an adverse effect on the anti-wear capacity of IL.

Regarding nanoparticles as powerful oil additives, different mechanisms, including rolling mechanism, self-repairing or mending mechanism, polishing mechanism and tribo-film formation, have been reported to explain the improvement on tribological performance of lubricants [17]. The most significant mechanism improving the tribological capability of the neat lubricant is tribofilm formation in two different ways: either nanoparticles are deposited and adsorbed on the sliding surfaces, or nanoparticles tribochemically react with the contact surface [17]. As a result of the Raman analysis reported, it is clear that this mechanism occurs in the case of the nanolubricants studied here, with h-BN nanoparticles being deposited and adsorbed on the sliding surfaces.

## 4. Conclusions

The synergistic effects of h-BN nanoparticles and three ILs as additives to PAO 32 base oil for a steel-steel contact at 298.15 K and 353.15 K were investigated. The three mixtures PAO 32 + IL and the three nanodispersions PAO 32 + IL + h-BN were stable for a minimum of 60 days, being the PAO 32 + IL1 + h-BN and PAO 32 + IL3 + h-BN stable for at least eight months.

The increase in the density of the base oil due to the addition of h-BN nanoparticles or/and ILs ranges from 0.06 % to 0.30 %. The viscosity of the base oil increases due to the addition of h-BN nanoparticles or/and ILs up to 7.0 %. The nanodispersion PAO 32 + IL2 + h-BN leads to maximum increases for both properties.

Using steel disks, corrosion tests of the three individual ILs indicated that the IL2 was only corrosive in room conditions whereas the absence of corrosion on the disk surface was observed when the sample was kept in an oven at 373.15 K for 24 hours continuously, showing that water content was the reason for poor anti-corrosion performance of IL2.

All the mixtures and nanodispersions improve both the antifriction and antiwear capabilities of PAO 32. The friction coefficient (COF) trend along time was quite stable with the addition of all the additives at 298.15 K in comparison with that at 353.15 K. At 298.15 K, a maximum friction reduction of 17 %, was achieved by the hybrid combination of 0.1 wt% h-BN and 1 wt% IL2 in the base oil, noting that their separate addition to PAO 32 decreased the COF to 8 % and 7 % for h-BN and IL2, respectively. At 353.15 K, the best friction-reduction performance was also achieved with the h-BN/IL2 hybrid additive, being the reduction 28 % compared with the neat oil. Accordingly, at high temperature, better synergy of h-BN/IL2 as hybrid additive for better friction reduction is obtained.

At 353.15 K, the best anti-wear performance was obtained with the hybrid combination of 0.1 wt% h-BN and 1 wt% IL1 with percentage reductions of 65 %, 97 %, 99 % and 92 % for the wear scar diameter, cross sectional area, wear volume and maximum depth of the wear scar, respectively.

It is interesting to note that at 353.15 K h-BN/IL3 hybrid additive improves the antifriction and antiwear performance of both separate additives, h-BN and IL3. Hence, positive synergies between h-BN and IL3 are clearly demonstrated.

As regards the roughness of the worn surfaces of the pins tested at 353.15 K, all the hybrid nanodispersions reduce this parameter in comparison with the neat oil, with the three PAO 32+IL mixtures and with the PAO 32+h-BN nanodispersion, for which the maximum roughness value was found.

Protective tribofilms formation on the worn surfaces tested at 353.15 K was revealed by Raman microscopy. From these results we can conclude that IL1 ($[P_{6,6,6,14}][DEHP]$) is a more

effective additive at boundary conditions than IL2 **(**[$P_{2,4,4,4}$][DEP]**)** or IL3 **(**[$P_{6,6,6,14}$][$(iC8)_2PO_2$]**)** since a lower presence in the corresponding tribofilm leads to a better antiwear performance.

## Acknowledgments

The authors acknowledge Repsol for providing us the PAO 32 sample. Authors would also thank RIAIDT-USC for the use of analytical facilities, especially to Mr. Ezequiel Vázquez for his useful advice. This work was supported by the Spanish Ministry of Science, Innovation and Universities and the ERDF programme (FEDER in Spanish) through ENE2017-86425-C2-2-R project, and by the Xunta de Galicia (ED431E 2018/08, ED431D 2017/06 and GRC ED431C 2016/001). These funders also financed the acquisition of the 3D Optical Profile (UNST15-DE-3156).

## 5. References


[1] Renewable Energy Statistics 2016. The International Renewable Energy Agency (IRENA), Abu Dhabi, 2016. https://www.irena.org/publications/2016/Jul/Renewable-Energy-Statistics-2016

[2] K. Solaun, E. Cerdá, Impacts of climate change on wind energy power – Four wind farms in Spain, Renewable Energy 145 (2020) 1306-1316. http://www.sciencedirect.com/science/article/pii/S0960148119309632

[3] A. Al-Dousari, W. Al-Nassar, A. Al-Hemoud, A. Alsaleh, A. Ramadan, N. Al-Dousari, M. Ahmed, Solar and wind energy: Challenges and solutions in desert regions, Energy 176 (2019) 184-194. http://www.sciencedirect.com/science/article/pii/S0360544219306000

[4] C.M.C.G. Fernandes, A.H. Battez, R. González, R. Monge, J.L. Viesca, A. García, R.C. Martins, J.H.O. Seabra, Torque loss and wear of FZG gears lubricated with wind turbine gear oils using an ionic liquid as additive, Tribol. Int. 90 (2015) 306-314. http://www.sciencedirect.com/science/article/pii/S0301679X15001899

[5] R. Monge, R. González, A. Hernández Battez, A. Fernández-González, J.L. Viesca, A. García, M. Hadfield, Ionic liquids as an additive in fully formulated wind turbine gearbox oils, Wear 328-329 (2015) 50-63. http://www.sciencedirect.com/science/article/pii/S0043164815000587

[6] M.A. Gutierrez, M. Haselkorn, P. Iglesias, The Lubrication Ability of Ionic Liquids as Additives for Wind Turbine Gearboxes Oils, Lubricants 4 (2016) 14. https://www.mdpi.com/2075-4442/4/2/14

[7] K. Michaelis, Influence factors on gearbox power loss, Ind. Lubr. Tribol. 63 (2011) 46-55. http://doi.org/10.1108/00368791111101830

[8] Y. Chen, P. Renner, H. Liang, Dispersion of Nanoparticles in Lubricating Oil: A Critical Review, Lubricants 7 (2019) 7. https://www.mdpi.com/2075-4442/7/1/7

[9] A.E. Somers, P.C. Howlett, D.R. MacFarlane, M. Forsyth, A Review of Ionic Liquid Lubricants, Lubricants 1 (2013) 3-21. http://www.mdpi.com/2075-4442/1/1/3

[10] M.F. Fox, M. Priest, Tribological properties of ionic liquids as lubricants and additives. Part 1: Synergistic tribofilm formation between ionic liquids and tricresyl phosphate, Proc. Inst. Mech. Eng. J 222 (2008) 291-303. http://journals.sagepub.com/doi/abs/10.1243/13506501JET387

[11] Y. Zhou, J. Qu, Ionic Liquids as Lubricant Additives: A Review, ACS Appl. Mater. Interfaces 9 (2017) 3209-3222. http://doi.org/10.1021/acsami.6b12489

[12] G. Paul, H. Hirani, T. Kuila, N.C. Murmu, Nanolubricants dispersed with graphene and its derivatives: an assessment and review of the tribological performance, Nanoscale 11 (2019) 3458-3483. http://dx.doi.org/10.1039/C8NR08240E

[13] S. Zhang, L. Ma, R. Dong, C.Y. Zhang, W.J. Sun, M.J. Fan, D.S. Yang, F. Zhou, W.M. Liu, Study on the synthesis and tribological properties of anti-corrosion benzotriazole ionic liquid, RSC Adv. 7 (2017) 11030-11040. http://dx.doi.org/10.1039/C6RA27376A

[14] S. Ko, C. Huh, Use of nanoparticles for oil production applications, J. Petrol. Sci. Eng. 172 (2019) 97-114. http://www.sciencedirect.com/science/article/pii/S0920410518308064

[15] I. Khan, K. Saeed, I. Khan, Nanoparticles: Properties, applications and toxicities, Arab. J. Chem. 12 (2019) 908-931. http://www.sciencedirect.com/science/article/pii/S1878535217300990

[16] W. Khalid Shafi, M.S. Charoo, NanoLubrication Systems: An Overview, Materials Today: Proceedings 5 (2018) 20621-20630. http://www.sciencedirect.com/science/article/pii/S2214785318315736

[17] N.F. Azman, S. Samion, Dispersion Stability and Lubrication Mechanism of Nanolubricants: A Review, Int. J. Precis Eng Manuf-Green Technol. 6 (2019) 393-414. http://doi.org/10.1007/s40684-019-00080-x
[18] V. Khare, M.-Q. Pham, N. Kumari, H.-S. Yoon, C.-S. Kim, J.-I.L. Park, S.-H. Ahn, Graphene–Ionic Liquid Based Hybrid Nanomaterials as Novel Lubricant for Low Friction and Wear, ACS Appl. Mater. Interfaces 5 (2013) 4063-4075. http://doi.org/10.1021/am302761c
[19] M.-D. Avilés, N. Saurín, J. Sanes, F.-J. Carrión, M.-D. Bermúdez, Ionanocarbon Lubricants. The Combination of Ionic Liquids and Carbon Nanophases in Tribology, Lubricants 5 (2017) 14. https://www.mdpi.com/2075-4442/5/2/14
[20] N. Saurín, M.D. Avilés, T. Espinosa, J. Sanes, F.J. Carrión, M.D. Bermúdez, P. Iglesias, Carbon nanophases in ordered nanofluid lubricants, Wear 376-377 (2017) 747-755. http://www.sciencedirect.com/science/article/pii/S0043164817300637
[21] J. Sanes, M.-D. Avilés, N. Saurín, T. Espinosa, F.-J. Carrión, M.-D. Bermúdez, Synergy between graphene and ionic liquid lubricant additives, Tribol. Int. 116 (2017) 371-382. http://doi.org/10.1016/j.triboint.2017.07.030
[22] Z. He, P. Alexandridis, Ionic liquid and nanoparticle hybrid systems: Emerging applications, Adv. Colloid Interface Sci. 244 (2017) 54-70. http://www.sciencedirect.com/science/article/pii/S0001868616302238
[23] X. Fan, L. Wang, High-performance lubricant additives based on modified graphene oxide by ionic liquids, J. Colloid Interf. Sci. 452 (2015) 98-108. http://www.sciencedirect.com/science/article/pii/S0021979715003914
[24] Y. Li, S. Zhang, Q. Ding, H. Li, B. Qin, L. Hu, Understanding the synergistic lubrication effect of 2-mercaptobenzothiazolate based ionic liquids and Mo nanoparticles as hybrid additives, Tribol. Int. 125 (2018) 39-45. http://www.sciencedirect.com/science/article/pii/S0301679X18302068
[25] J.M. Liñeira del Río, E.R. López, J. Fernández, Synergy between boron nitride or graphene nanoplatelets and tri(butyl)ethylphosphonium diethylphosphate ionic liquid as lubricant additives of triisotridecyltrimellitate oil, J. Mol. Liq. 301 (2020) 112442. http://www.sciencedirect.com/science/article/pii/S0167732219354443
[26] B.T. Seymour, W. Fu, R.A.E. Wright, H. Luo, J. Qu, S. Dai, B. Zhao, Improved Lubricating Performance by Combining Oil-Soluble Hairy Silica Nanoparticles and an Ionic Liquid as an Additive for a Synthetic Base Oil, ACS Appl. Mater. Interfaces 10 (2018) 15129-15139. http://doi.org/10.1021/acsami.8b01579
[27] M. Upendra, V. Vasu, Synergistic Effect Between Phosphonium-Based Ionic Liquid and Three Oxide Nanoparticles as Hybrid Lubricant Additives, J. Tribol. 142 (2020) 052101. http://doi.org/10.1115/1.4045769
[28] S.A.S. Amiril, E. Rahim, N. Talib, K. Kamdani, M. Rahim, S. Samion, Performance Evaluation of Palm-Olein TMP Ester Containing Hexagonal Boron Nitride and an Oil Miscible Ionic Liquid as Bio-Based Metalworking Fluids, J. Mech. Eng. SI 4 (2017) 223-234. http://jmeche.uitm.edu.my/wp-content/uploads/bsk-pdf-manager/P17_ID_169_162.pdf
[29] J.M. Liñeira del Río, M.J.G. Guimarey, M.J.P. Comuñas, E.R. López, J.I. Prado, L. Lugo, J. Fernández, Thermophysical and tribological properties of environmentally-friendly lubricants based on trimethylolpropane trioleate with hexagonal boron nitride nanoparticles as additive, Coatings 9 (2019) 509. http://doi.org/10.3390/coatings9080509
[30] G.M. Ay, Y. Göncü, N. Ay, Environmentally friendly material: Hexagonal boron nitride, Journal of Boron 1 (2016) 66-73. http://dergipark.org.tr/en/download/article-file/226224
[31] I. Otero, E.R. López, M. Reichelt, M. Villanueva, J. Salgado, J. Fernández, Ionic liquids based on phosphonium cations as neat lubricants or lubricant additives for a steel/steel

654 contact, ACS Appl. Mater. Interfaces 6 (2014) 13115-13128.
655 http://dx.doi.org/10.1021/am502980m
656 [32] D. Coronado, J. Wenske, Monitoring the Oil of Wind-Turbine Gearboxes: Main
657 Degradation Indicators and Detection Methods, Machines 6 (2018) 25.
658 https://www.mdpi.com/2075-1702/6/2/25
659 [33] C. Sequeira, A. Pacheco, P. Galego, E. Gorbeña, Analysis of the efficiency of wind turbine
660 gearboxes using the temperature variable, Renewable Energy 135 (2019) 465-472.
661 http://www.sciencedirect.com/science/article/pii/S096014811831471X
662 [34] R.J. de Andrade Vieira, M.Á. Sanz Bobi, Evaluación de Indicadores de la Condición de
663 Aerogeneradores, Anales de Mecánica y Electricidad 90 (2013) 17-26.
664 https://www.iit.comillas.edu/docs/IIT-13-030A.pdf
665 [35] M.J.G. Guimarey, M.J.P. Comuñas, E.R. López, A. Amigo, J. Fernández, Thermophysical
666 properties of polyalphaolefin oil modified with nanoadditives, J. Chem. Thermodyn.
667 131 (2019) 192-205.
668 http://www.sciencedirect.com/science/article/pii/S0021961418307973
669 [36] R. González, A.H. Battez, J.L. Viesca, A. Higuera-Garrido, A. Fernández-González,
670 Lubrication of DLC Coatings with Two Tris(pentafluoroethyl)trifluorophosphate Anion-
671 Based Ionic Liquids, Tribol. Trans. 56 (2013) 887-895.
672 http://doi.org/10.1080/10402004.2013.810319
673 [37] A. Ramírez-Hernández, C. Aguilar-Flores, A. Aparicio-Saguilán, Fingerprint analysis of FTIR
674 spectra of polymers containing vinyl acetate, DYNA 86 (2019) 198-205.
675 http://doi.org/10.15446/dyna.v86n209.77513
676 [38] J.M. Liñeira del Río, E.R. López, J. Fernández, F. García, Tribological properties of
677 dispersions based on reduced graphene oxide sheets and trimethylolpropane trioleate
678 or PAO 40 oils, J. Mol. Liq. 274 (2019) 568-576.
679 http://www.sciencedirect.com/science/article/pii/S0167732218339230
680 [39] A. Hernández Battez, M. Bartolomé, D. Blanco, J.L. Viesca, A. Fernández-González, R.
681 González, Phosphonium cation-based ionic liquids as neat lubricants: Physicochemical
682 and tribological performance, Tribol. Int. 95 (2016).
683 http://doi.org/10.1016/j.triboint.2015.11.015
684 [40] H. Danjo, W. Sasaki, T. Miyazaki, T. Imamoto, P-Chirogenic phosphonium salts:
685 preparation and use in Rh-catalyzed asymmetric hydrogenation of enamides,
686 Tetrahedron Lett. 44 (2003) 3467-3469.
687 http://www.sciencedirect.com/science/article/pii/S0040403903006683
688 [41] M. Praveena, K. Guha, A. Ravishankar, S.K. Biswas, C.D. Bain, V. Jayaram, Total internal
689 reflection Raman spectroscopy of poly(alpha-olefin) oils in a lubricated contact, RSC
690 Adv. 4 (2014) 22205-22213. http://dx.doi.org/10.1039/C4RA02261K
691 [42] H. Okubo, C. Tadokoro, Y. Hirata, S. Sasaki, In Situ Raman Observation of the
692 Graphitization Process of Tetrahedral Amorphous Carbon Diamond-Like Carbon under
693 Boundary Lubrication in Poly-Alpha-Olefin with an Organic Friction Modifier, Tribology
694 Online 12 (2017) 229-237. http://doi.org/10.2474/trol.12.229
695 [43] Q. Wan, Y. Jin, P. Sun, Y. Ding, Tribological Behaviour of a Lubricant Oil Containing Boron
696 Nitride Nanoparticles, Procedia Eng. 102 (2015) 1038-1045.
697 http://www.sciencedirect.com/science/article/pii/S1877705815002453
698 [44] M.-D. Bermúdez, A.-E. Jiménez, J. Sanes, F.-J. Carrión, Ionic liquids as advanced lubricant
699 fluids, Molecules 14 (2009) 2888-2908.
700 https://www.ncbi.nlm.nih.gov/pmc/articles/PMC6255031/
701 [45] X. Paredes, O. Fandiño, M.J.P. Comuñas, A.S. Pensado, J. Fernández, Study of the effects of
702 pressure on the viscosity and density of diisodecyl phthalate, J. Chem. Thermodyn. 41
703 (2009) 1007-1015.
704 http://www.sciencedirect.com/science/article/pii/S002196140900072X

[46] F.M. Gaciño, T. Regueira, L. Lugo, M.J.P. Comuñas, J. Fernández, Influence of Molecular Structure on Densities and Viscosities of Several Ionic Liquids, J. Chem. Eng. Data 56 (2011) 4984-4999. http://doi.org/10.1021/je200883w
[47] P. Heyer, J. Läuger, Correlation between friction and flow of lubricating greases in a new tribometer device, Lubr. Sci. 21 (2009) 253-268. http://onlinelibrary.wiley.com/doi/abs/10.1002/ls.88
[48] F. Moreira-Izurieta, A. Jabbarzadeh, Tribological studies in cartilaginous tissue of lamb synovial joints lubricated by distilled water and interstitial-fluid-like solution, Tribology in Industry 39 (2017) 319-328. http://www.tribology.fink.rs/journals/2017/2017-3/2017-3-06.html
[49] A. He, S. Huang, J.-H. Yun, H. Wu, Z. Jiang, J. Stokes, S. Jiao, L. Wang, H. Huang, Tribological Performance and Lubrication Mechanism of Alumina Nanoparticle Water-Based Suspensions in Ball-on-Three-Plate Testing, Tribol. Lett. 65 (2017) 40. https://doi.org/10.1007/s11249-017-0823-y
[50] A. Beheshti, Y. Huang, K. Ohno, I. Blakey, J.R. Stokes, Improving tribological properties of oil-based lubricants using hybrid colloidal additives, Tribol. Int. 144 (2020) 106130. http://www.sciencedirect.com/science/article/pii/S0301679X19306449
[51] B.J. Hamrock, D. Dowson, Isothermal Elastohydrodynamic Lubrication of Point Contacts: Part III—Fully Flooded Results, Journal of Lubrication Technology 99 (1977) 264-275. http://doi.org/10.1115/1.3453074
[52] N. Ohno, W. Tokunaga, S. Mia, Prediction of Pressure-Viscosity Coefficient Based on Sound Velocity of Lubricating Oils, AUSTRIB 06, Brisbane, Australia (2006).
[53] Y. Xu, Y. Peng, K.D. Dearn, T. You, J. Geng, X. Hu, Fabrication and tribological characterization of laser textured boron cast iron surfaces, Surf. Coat. Technol. 313 (2017) 391-401. http://www.sciencedirect.com/science/article/pii/S0257897217301470
[54] S. Kawada, S. Watanabe, R. Tsuboi, S. Sasaki, B. Prakash, Lubrication Mechanism of Halogen-Free Ionic Liquids, Tribology Online 12 (2017) 155-161. http://doi.org/10.2474/trol.12.155
[55] J. Zhang, Y. Meng, Boundary lubrication by adsorption film, Friction 3 (2015) 115-147. http://doi.org/10.1007/s40544-015-0084-4
[56] M. Ratoi, H. Tanaka, B.G. Mellor, J. Sugimura, Hydrocarbon Lubricants Can Control Hydrogen Embrittlement, Scientific Reports 10 (2020) 1361. http://doi.org/10.1038/s41598-020-58294-y
[57] H. Li, A.E. Somers, P.C. Howlett, M.W. Rutland, M. Forsyth, R. Atkin, Addition of low concentrations of an ionic liquid to a base oil reduces friction over multiple length scales: a combined nano- and macrotribology investigation, Phys. Chem. Chem. Phys. 18 (2016) 6541-6547. http://dx.doi.org/10.1039/C5CP07061A
[58] S. Cowie, P.K. Cooper, R. Atkin, H. Li, Nanotribology of Ionic Liquids as Lubricant Additives for Alumina Surfaces, The Journal of Physical Chemistry C 121 (2017) 28348-28353. http://doi.org/10.1021/acs.jpcc.7b09879
[59] A.E. Somers, B. Khemchandani, P.C. Howlett, J. Sun, D.R. MacFarlane, M. Forsyth, Ionic Liquids as Antiwear Additives in Base Oils: Influence of Structure on Miscibility and Antiwear Performance for Steel on Aluminum, ACS Appl. Mater. Interfaces 5 (2013) 11544-11553. http://doi.org/10.1021/am4037614

**Supplementary Material**

# Synergistic effects of hexagonal boron nitride nanoparticles and phosphonium ionic liquids as hybrid lubricant additives

**Khodor I. Nasser, José M. Liñeira del Río, Enriqueta R. López*, Josefa Fernández**

Laboratory of Thermophysical Properties, Nafomat Group, Department of Applied Physics, Faculty of Physics, University of Santiago de Compostela, 15782, Santiago de Compostela, Spain

*Corresponding author.

E-mail address: enriqueta.lopez@usc.es

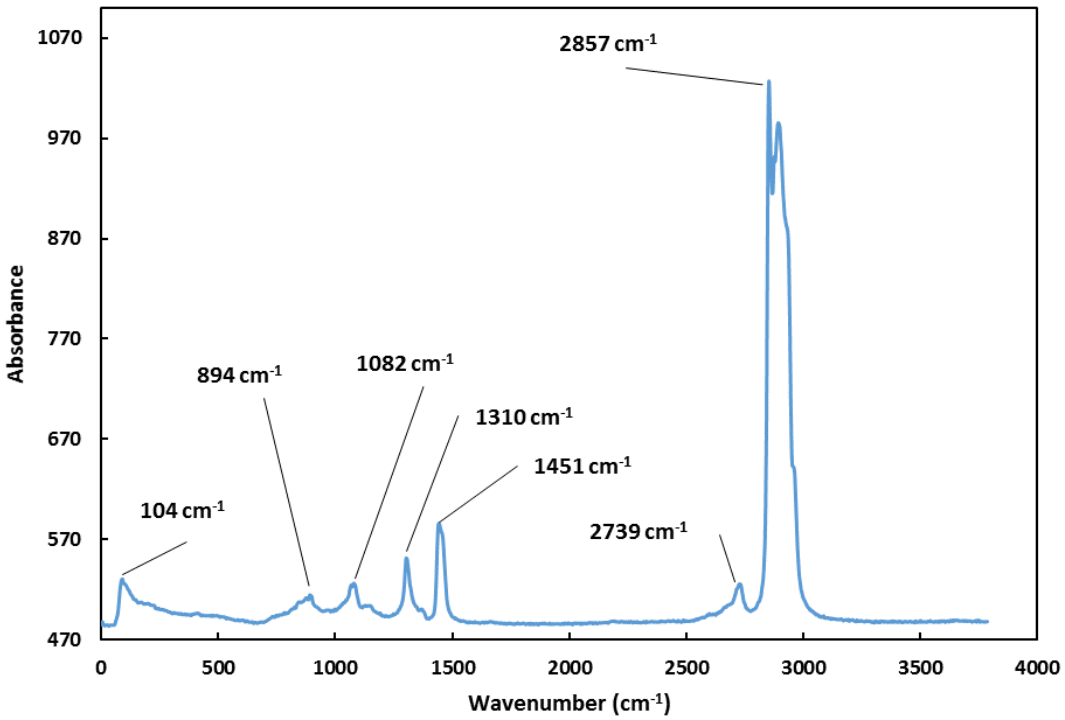


774

775 **Fig. S1.** Raman spectrum of PAO 32

776

777

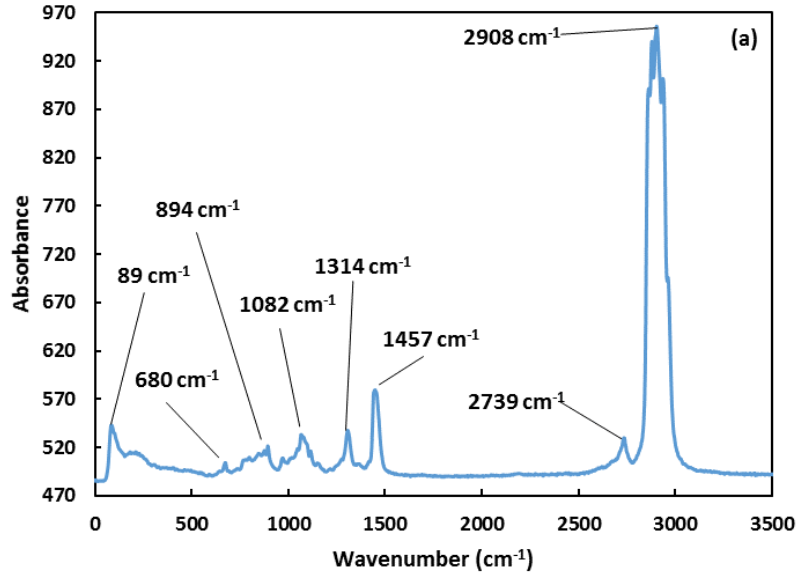


778

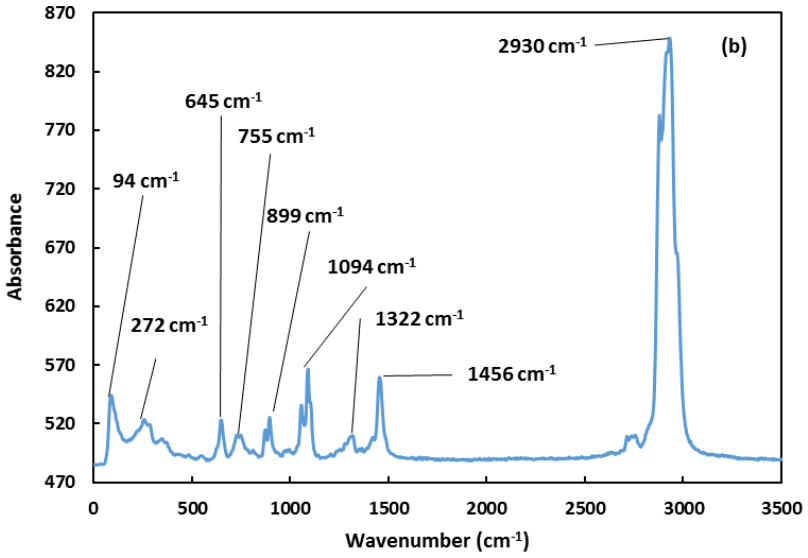


779

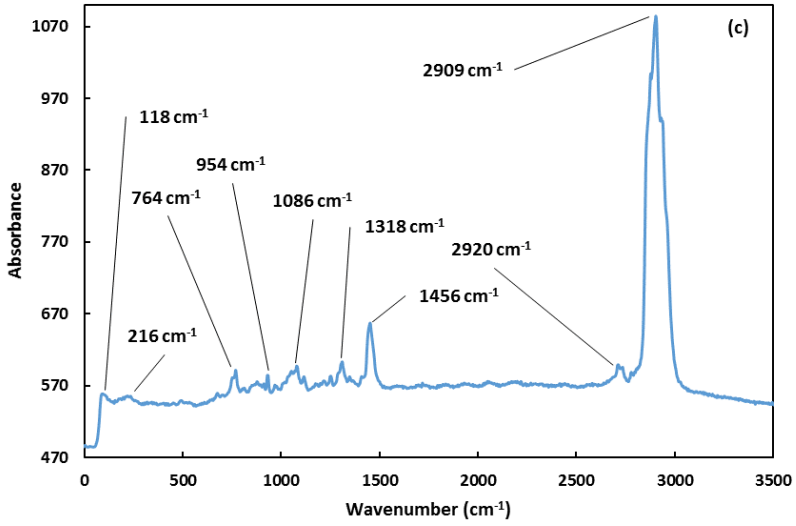


780

781 **Fig. S2.** Raman spectra of: (a) IL1, (b) IL2 and (c) IL3

782

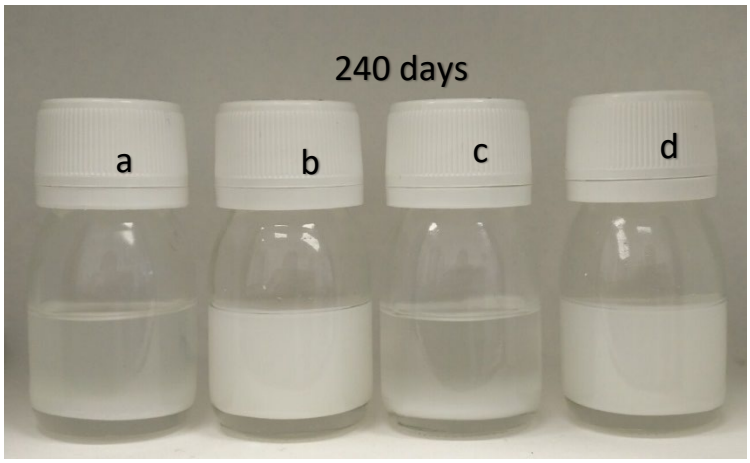


**Fig. S3.** Photographs used for assigning the stability of the nanodispersions: (a) PAO 32 + 0.1 wt% h-BN, (b) PAO 32 + 1 wt% IL1 + 0.1 wt% h-BN, (c) PAO 32 + 1 wt% IL2 + 0.1 wt% h-BN, (d) PAO 32 + 1 wt% IL3 + 0.1 wt% h-BN.

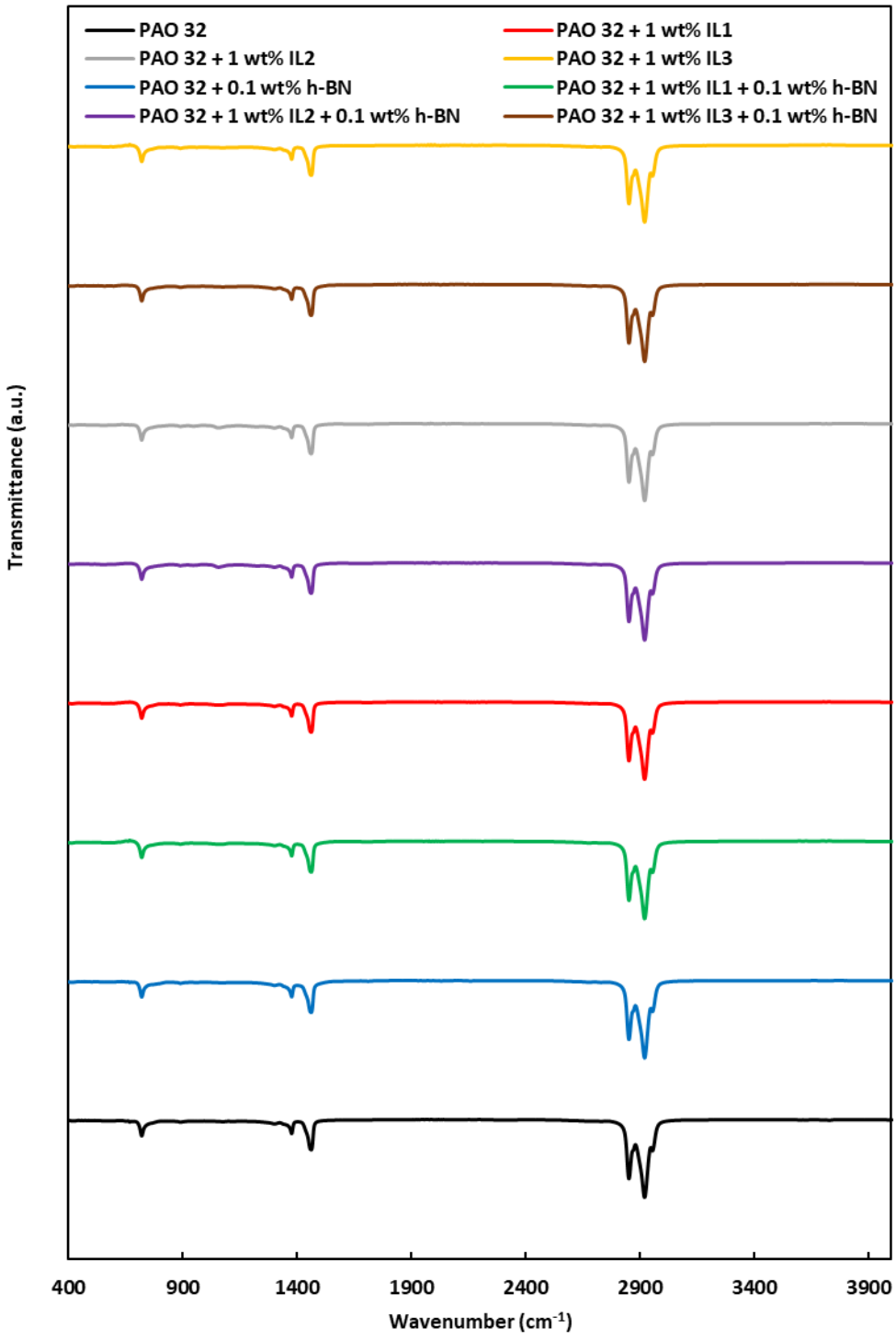


788

789 **Fig. S4.** FTIR spectra of all the samples

790

791

**Table S1**

Density ($\rho$, g/cm$^3$) of the PAO 32 oil, its mixtures and dispersions as a function of temperature at 0.1 MPa

| | PAO 32 | PAO 32 + 1 wt% IL1 | PAO 32 + 1 wt% IL2 | PAO 32 + 1 wt% IL3 | PAO 32 + 0.1 wt% h-BN | PAO 32 + 1 wt% IL1+ 0.1 wt% h-BN | PAO 32 + 1 wt% IL2+ 0.1 wt% h-BN | PAO 32 + 1 wt% IL3+ 0.1 wt% h-BN |
|---|---|---|---|---|---|---|---|---|
| Temperature(K) | ρ(g/cm$^3$) | ρ(g/cm$^3$) | ρ(g/cm$^3$) | ρ(g/cm$^3$) | ρ(g/cm$^3$) | ρ(g/cm$^3$) | ρ(g/cm$^3$) | ρ(g/cm$^3$) |
| 278.15 | 0.8522 | 0.8534 | 0.8539 | 0.8532 | 0.8531 | 0.8541 | 0.8547 | 0.8531 |
| 283.15 | 0.8492 | 0.8505 | 0.851 | 0.8503 | 0.8501 | 0.8511 | 0.8517 | 0.8503 |
| 288.15 | 0.8463 | 0.8475 | 0.848 | 0.8473 | 0.8472 | 0.8482 | 0.8488 | 0.8474 |
| 293.15 | 0.8433 | 0.8446 | 0.8451 | 0.8444 | 0.8442 | 0.8452 | 0.8458 | 0.8445 |
| 298.15 | 0.8403 | 0.8416 | 0.8421 | 0.8414 | 0.8412 | 0.8422 | 0.8428 | 0.8416 |
| 303.15 | 0.8374 | 0.8386 | 0.8391 | 0.8384 | 0.8383 | 0.8392 | 0.8399 | 0.8387 |
| 308.15 | 0.8344 | 0.8357 | 0.8362 | 0.8354 | 0.8353 | 0.8363 | 0.8369 | 0.8358 |
| 313.15 | 0.8315 | 0.8327 | 0.8333 | 0.8325 | 0.8324 | 0.8333 | 0.8340 | 0.8329 |
| 318.15 | 0.8286 | 0.8298 | 0.8303 | 0.8295 | 0.8295 | 0.8304 | 0.8310 | 0.8299 |
| 323.15 | 0.8257 | 0.8268 | 0.8274 | 0.8266 | 0.8265 | 0.8274 | 0.8280 | 0.8270 |
| 328.15 | 0.8227 | 0.8239 | 0.8244 | 0.8236 | 0.8236 | 0.8244 | 0.8251 | 0.8241 |
| 333.15 | 0.8198 | 0.8209 | 0.8215 | 0.8206 | 0.8206 | 0.8215 | 0.8221 | 0.8211 |
| 338.15 | 0.8169 | 0.8180 | 0.8185 | 0.8177 | 0.8177 | 0.8185 | 0.8191 | 0.8182 |
| 343.15 | 0.8139 | 0.8150 | 0.8156 | 0.8147 | 0.8147 | 0.8155 | 0.8162 | 0.8152 |
| 348.15 | 0.8110 | 0.8120 | 0.8126 | 0.8117 | 0.8117 | 0.8125 | 0.8132 | 0.8122 |
| 353.15 | 0.8080 | 0.8090 | 0.8096 | 0.8087 | 0.8088 | 0.8096 | 0.8102 | 0.8093 |
| 358.15 | 0.8051 | 0.8060 | 0.8066 | 0.8057 | 0.8058 | 0.8066 | 0.8072 | 0.8063 |
| 363.15 | 0.8021 | 0.8030 | 0.8036 | 0.8027 | 0.8028 | 0.8036 | 0.8042 | 0.8033 |
| 368.15 | 0.7992 | 0.8000 | 0.8007 | 0.7997 | 0.7998 | 0.8006 | 0.8012 | 0.8003 |
| 373.15 | 0.7963 | 0.7971 | 0.7977 | 0.7968 | 0.7968 | 0.7976 | 0.7982 | 0.7973 |

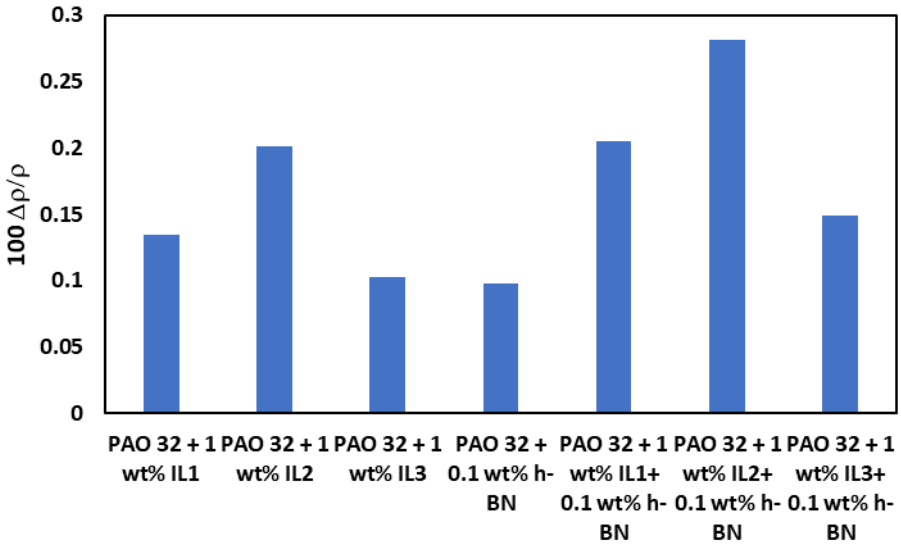


**Fig. S5.** Percentage mean relative density increase ($\Delta\rho/\rho$) from 278.15 K to 373.15 K of the mixtures and nanodispersions containing PAO 32

**Table S2**

Dynamic viscosity ($\eta$, mPa·s), of the PAO 32 oil, its mixtures and dispersions as a function of temperature

| | PAO 32 | PAO 32 + 1 wt% IL1 | PAO 32 + 1 wt% IL2 | PAO 32 + 1 wt% IL3 | PAO 32 + 0.1 wt% h-BN | PAO 32 + 1 wt% IL1+ 0.1 wt% h-BN | PAO 32 + 1 wt% IL2+ 0.1 wt% h-BN | PAO 32 + 1 wt% IL3+ 0.1 wt% h-BN |
|---|---|---|---|---|---|---|---|---|
| **Temperature(K)** | η(mPa.s) | η(mPa.s) | η(mPa.s) | η(mPa.s) | η(mPa.s) | η(mPa.s) | η(mPa.s) | η(mPa.s) |
| **278.15** | 2230 | 2294 | 2381 | 2285 | 2270 | 2301 | 2387 | 2311 |
| **283.15** | 1514 | 1556 | 1611 | 1551 | 1540 | 1562 | 1618 | 1568 |
| **288.15** | 1054 | 1084 | 1121 | 1081 | 1073 | 1088 | 1126 | 1092 |
| **293.15** | 752.0 | 773.1 | 798.4 | 770.6 | 765.4 | 775.9 | 801.1 | 778.8 |
| **298.15** | 548.0 | 562.7 | 580.5 | 561.1 | 557.3 | 564.7 | 582.1 | 566.8 |
| **303.15** | 406.6 | 417.5 | 430.2 | 416.3 | 413.7 | 419.0 | 431.1 | 420.5 |
| **308.15** | 307.2 | 315.2 | 324.4 | 314.4 | 321.5 | 316.3 | 325.8 | 317.4 |
| **313.15** | 236.0 | 241.9 | 248.7 | 241.3 | 239.9 | 242.7 | 249.9 | 243.4 |
| **318.15** | 184.0 | 188.4 | 193.5 | 187.9 | 187.0 | 189.0 | 194.6 | 189.5 |
| **323.15** | 145.4 | 149.0 | 152.6 | 148.4 | 147.7 | 149.3 | 153.6 | 149.6 |
| **328.15** | 116.3 | 119.1 | 122.0 | 118.8 | 118.8 | 119.4 | 122.8 | 119.6 |
| **333.15** | 94.28 | 96.45 | 98.67 | 96.19 | 95.84 | 96.70 | 99.42 | 96.82 |
| **338.15** | 77.23 | 78.97 | 80.71 | 78.76 | 78.59 | 79.20 | 81.35 | 79.26 |
| **343.15** | 63.92 | 65.35 | 66.72 | 65.17 | 65.02 | 65.57 | 67.25 | 65.56 |
| **348.15** | 53.43 | 54.60 | 55.67 | 54.45 | 54.36 | 54.79 | 56.15 | 54.80 |
| **353.15** | 44.92 | 46.05 | 46.88 | 45.96 | 45.86 | 46.18 | 47.31 | 46.17 |
| **358.15** | 38.01 | 39.09 | 39.82 | 38.99 | 39.09 | 39.26 | 40.14 | 39.19 |
| **363.15** | 32.54 | 33.48 | 34.10 | 33.41 | 33.47 | 33.67 | 34.36 | 33.58 |
| **368.15** | 28.23 | 28.88 | 29.40 | 28.83 | 28.92 | 29.10 | 29.64 | 28.97 |
| **373.15** | 25.01 | 25.08 | 25.51 | 25.04 | 25.15 | 25.27 | 25.72 | 25.16 |

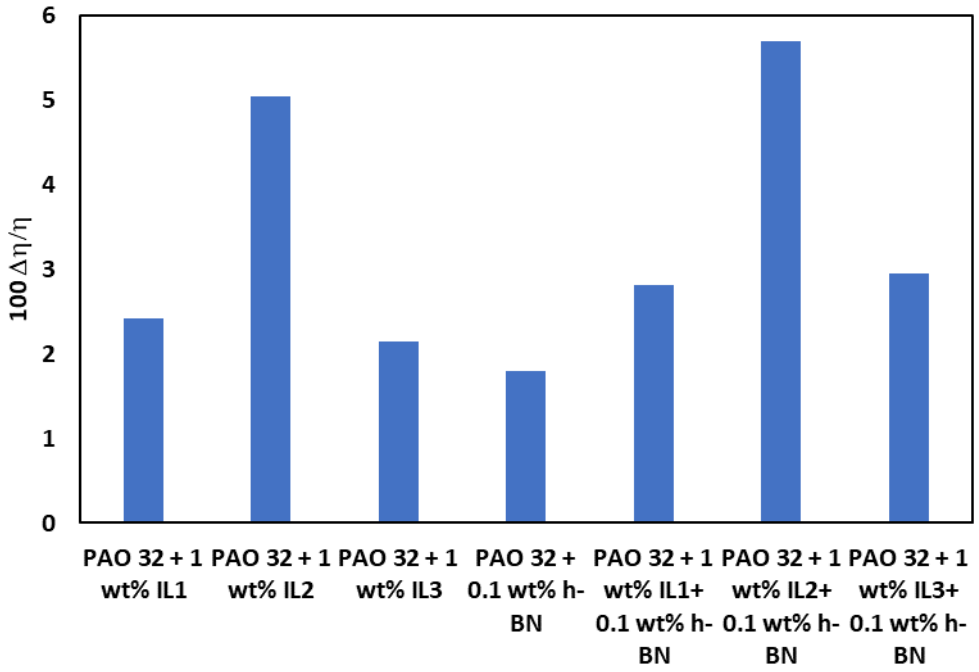


**Fig. S6.** Percentage mean relative dynamic viscosity increase ($\Delta\eta/\eta$) from 278.15 K to 373.15 K of the mixtures and nanodispersions containing PAO 32

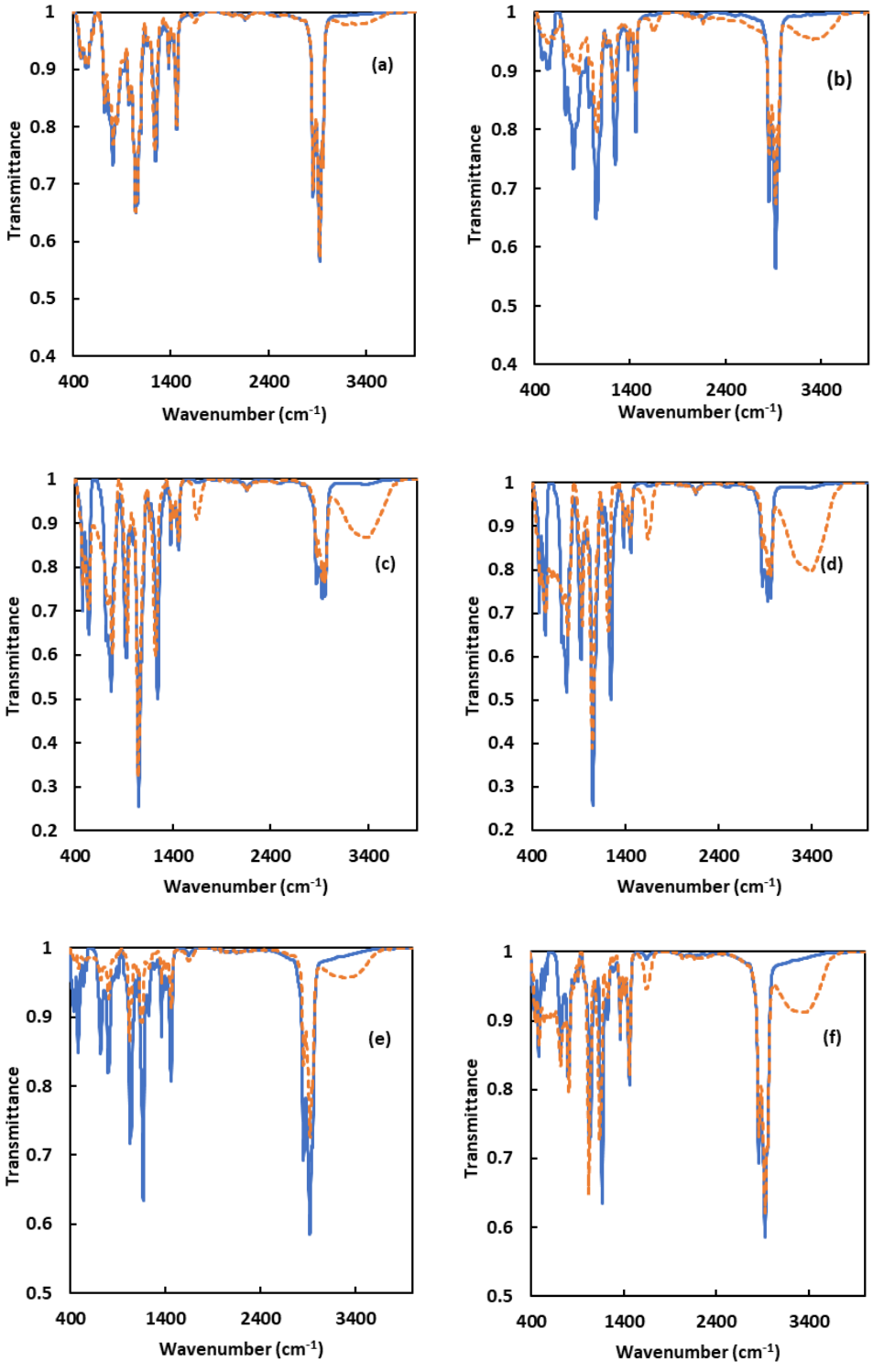


**Fig. S7.** infrared spectra of ILs : (a) (–) IL1 fresh sample, (–) IL1 collected from the disk after 24 hours in a 373 K oven; (b) (–) IL1 fresh sample, (–) IL1 collected from the disk after 35 days of surface contact; (c) (–) IL2 fresh sample, (–) IL2 collected from the disk after 24 hours in a 373 K oven; (d) (–) IL2 fresh sample, (–) IL2 collected from the disk after 35 days of surface contact; (e) (–) IL3 fresh sample, (–) IL3 collected from the disk after 24 hours in a 373 K oven; (f) (–) IL3 fresh sample, (–) IL3 collected from the disk after 35 days of surface contact;

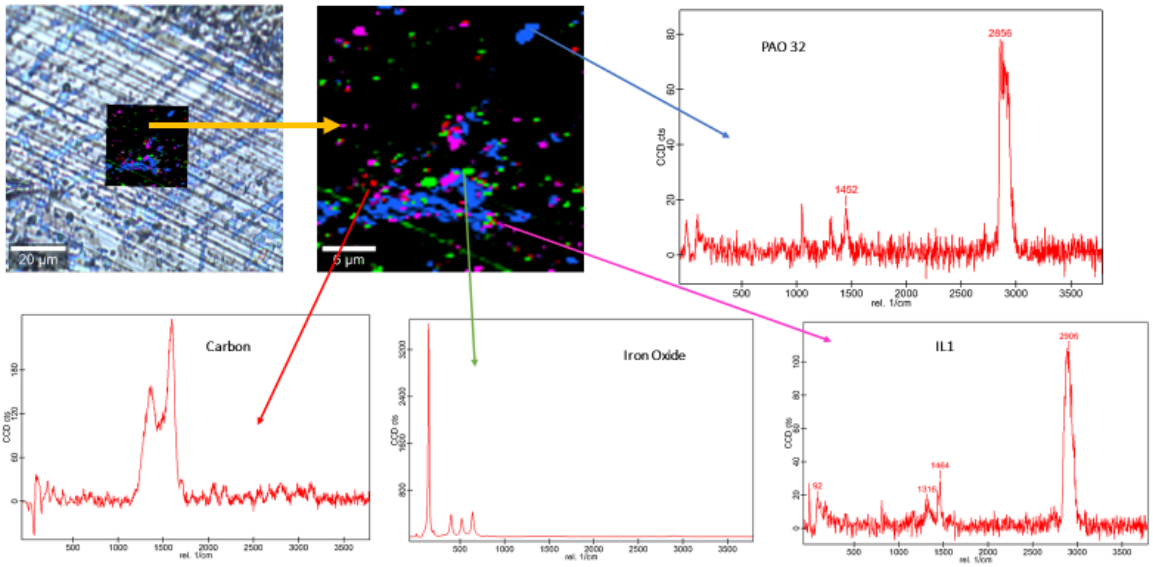


**Fig. S8.** RAMAN Spectra and element map combination at the worn surface lubricated by: PAO 32 + 1 wt% IL1 at 353.15 K

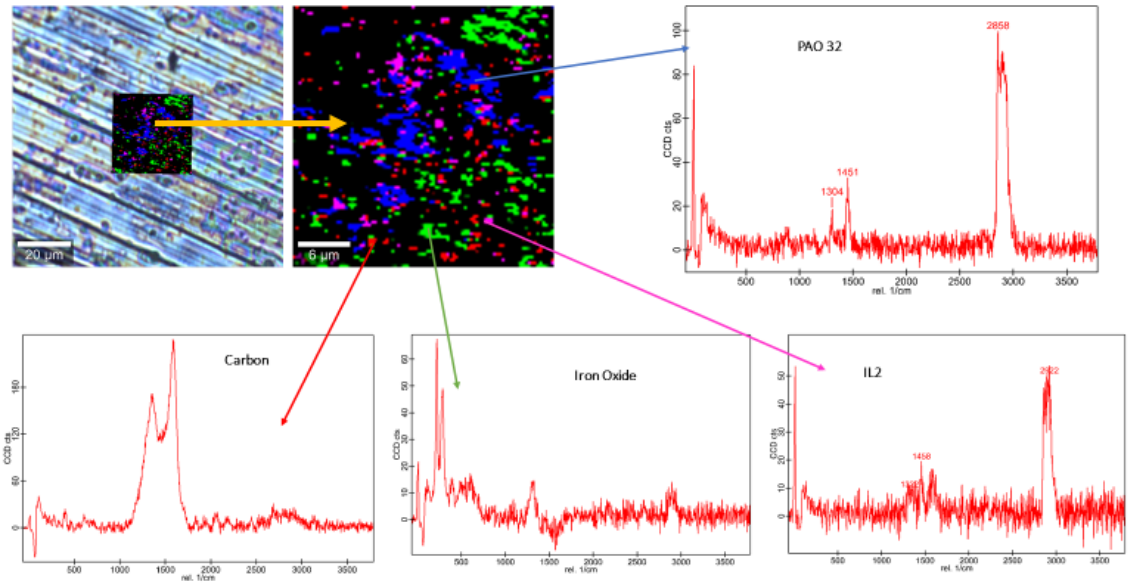


**Fig. S9.** RAMAN Spectra and element map combination at the worn surface lubricated by: PAO 32 + 1 wt% IL2 at 353.15 K

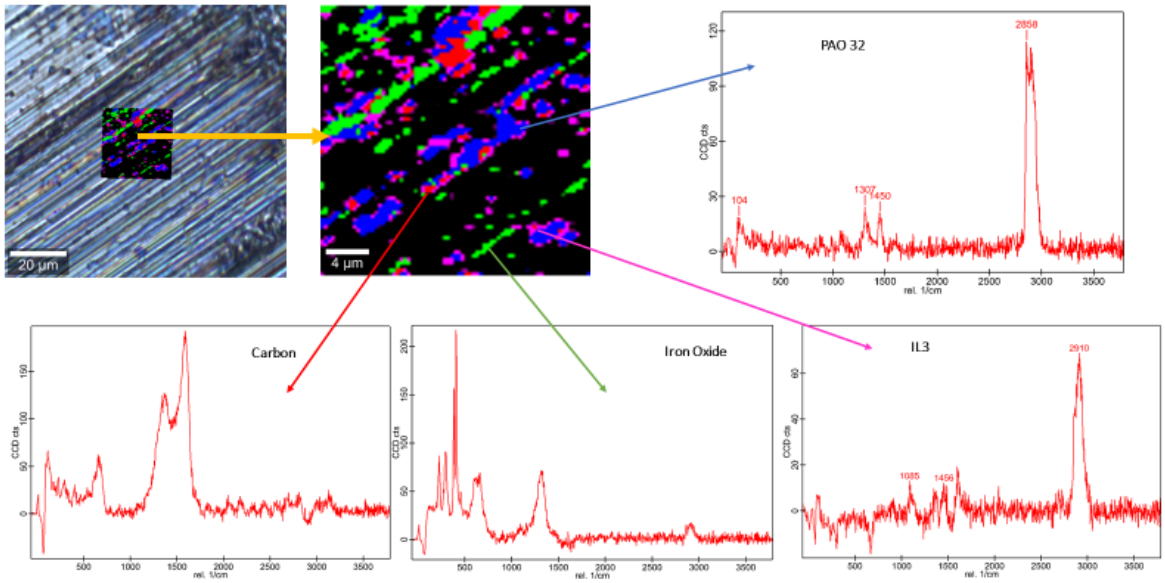


**Fig. S10.** RAMAN Spectra and element map combination at the worn surface lubricated by: PAO 32 + 1 wt% IL3 at 353.15 K

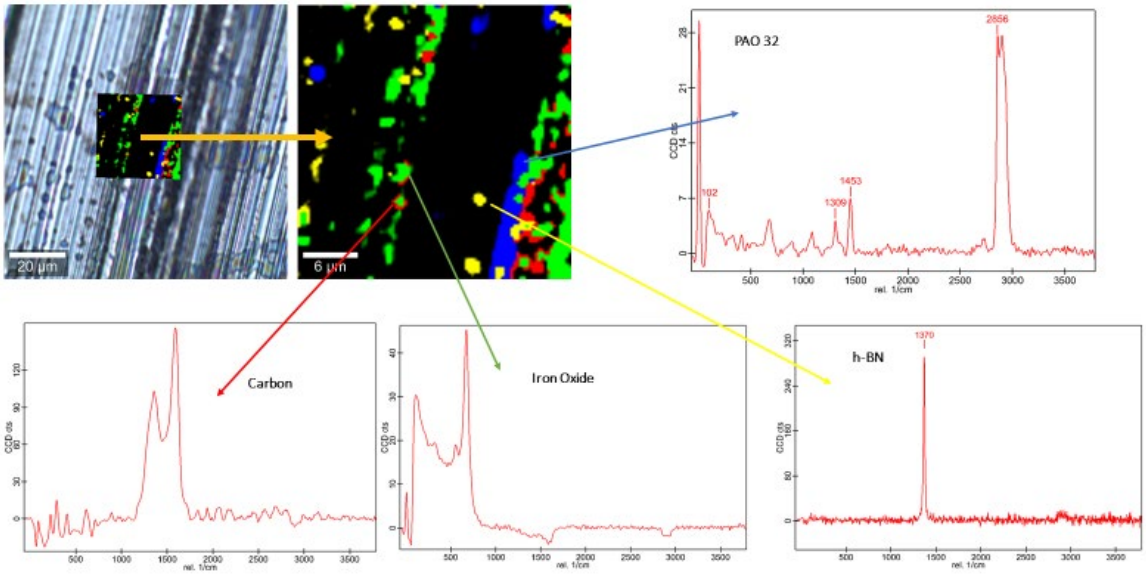


**Fig. S11.** RAMAN Spectra and element map combination at the worn surface lubricated by: PAO 32 + 0.1 wt% h-BN at 353.15 K

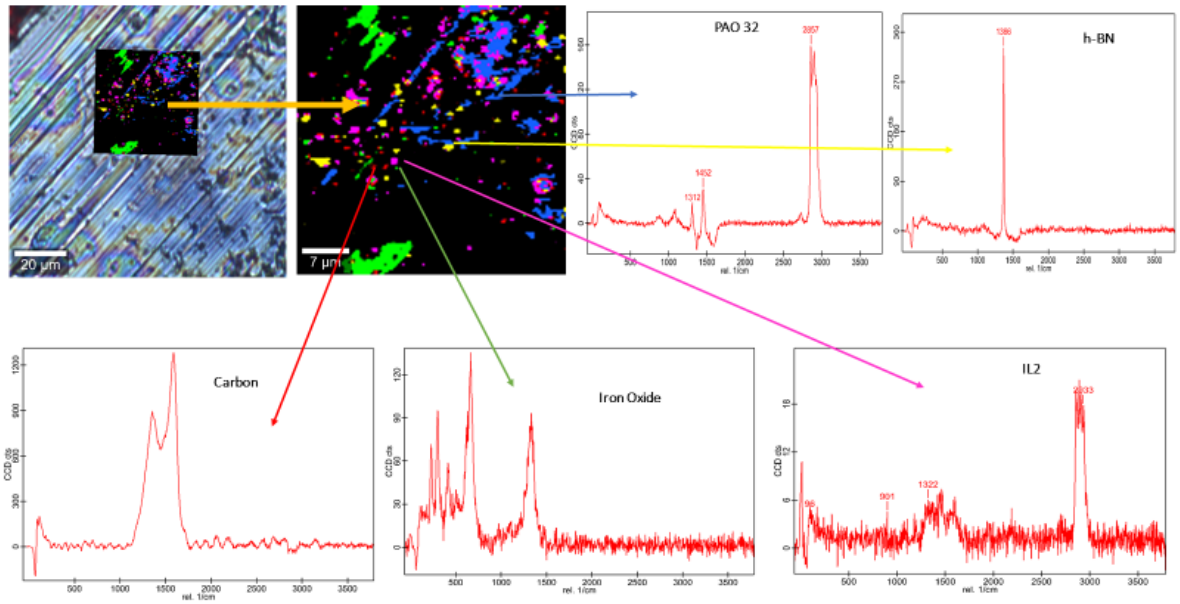


**Fig. S12.** RAMAN Spectra and element map combination at the worn surface lubricated by: PAO 32 + 1 wt% IL2+ 0.1 wt% h-BN at 353.15 K

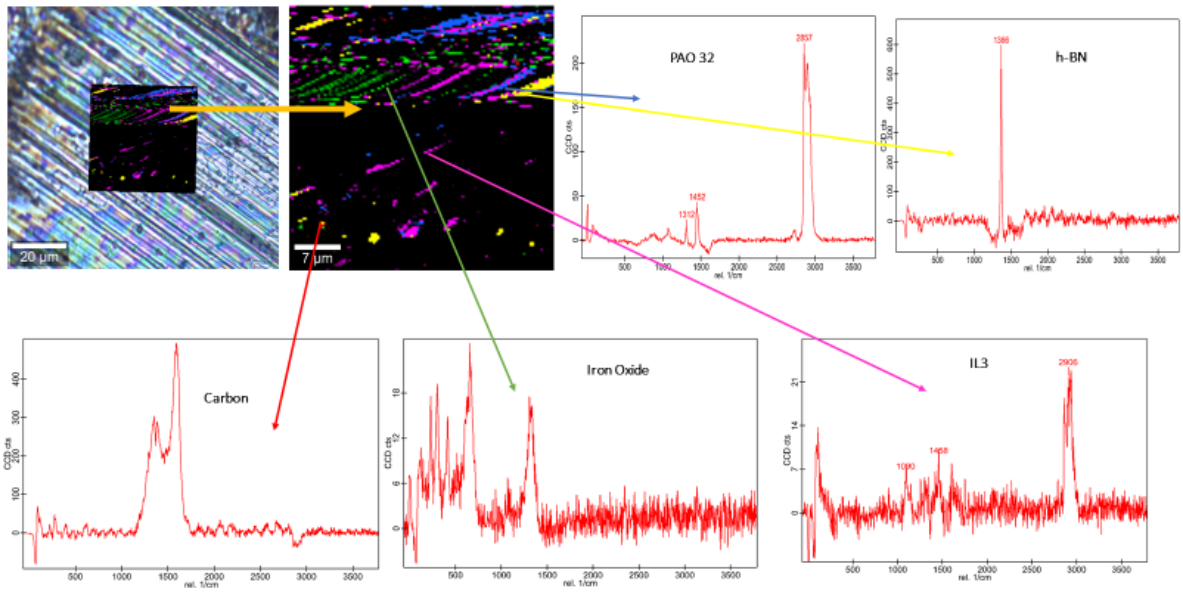


**Fig. S13.** RAMAN Spectra and element map combination at the worn surface lubricated by: PAO 32 + 1 wt% IL3+ 0.1 wt% h-BN at 353.15 K